

## Electromagnetic and hadronic interaction form factors for the ground, $(\frac{3}{2}^-\frac{1}{2})_1$ and $(\frac{3}{2}^-\frac{3}{2})_1$ states in $^{13}\text{C}$ and $^{13}\text{N}$

K. Amos, L. Berge, and D. Kurath\*

*School of Physics, The University of Melbourne, Parkville, Victoria 3052, Australia*

(Received 31 October 1988)

The  $\beta$ - and  $\gamma$ -decay rates, electron scattering form factors, and intermediate energy ( $p, p'$ ) and ( $p, n$ ) cross-section data from select transitions in  $^{13}\text{C}$  and  $^{13}\text{N}$  are analyzed to test  $0p$  shell-model predictions of  $M1$  components of the spin-flip transition densities, and to quantitatively assess magnetic dipole quenching.

### I. INTRODUCTION

There has been a flurry of activity<sup>1-6</sup> in the measurement and analysis of charge-exchange ( $p, n$ ) data from  $0p$  shell nuclei. This was motivated by the empirical proportionality<sup>2</sup> that relates the zero-momentum-transfer ( $p, n$ ) cross sections to Fermi and/or Gamow-Teller  $\beta$ -decay strengths. But extraction of  $B_F$  and  $B_{GT}$  from the  $0^\circ$  ( $p, n$ ) data relies upon a sufficient knowledge of reaction mechanism and nuclear structure details. At the very least, for all analyses made to date, the impulse approximation must be valid and renormalizations between calculated and measured values due to inadequacies of nuclear structure must be the same for ( $p, n$ ) data as well as for  $\beta$  decay.<sup>3</sup>

These recent studies of ( $p, n$ ) data have been taken with proton energies varying from 135 to 800 MeV, and as such, satisfy basic criteria for the impulse approximation to be valid. But most are concerned only with the  $0^\circ$  scattering cross sections and use one or more of a sequence of simplifying approximations in their analyses. Approximations such as ignoring medium correction effects in the two-nucleon  $t$  matrix, especially at 135-200 MeV incident energy, using only the central force component of the  $t$  matrix; adjusting oscillator lengths excessively to achieve a best fit to data, and ignoring altogether, or at best, using a poor approximation to, the exact exchange amplitudes that arise from proper antisymmetrizations of the complete scattering system, are commonly used.

But irrespective of errors introduced into data analyses by using any or all of the approximations specified, renormalization scales assessed by  $0^\circ$  data studies lose significance if the model fails to reproduce data at other momentum-transfer (scattering angle) values. Indeed, in the most recent of the ( $p, n$ ) studies,<sup>4</sup> momentum-transfer variation of data was considered and, from which it is clear, medium corrections to the two-nucleon  $t$  matrix are very important, especially for data taken with projectile energies below 200 MeV. Horowitz<sup>7</sup> suggests that such effects persist strongly to even higher incident energies. But his study used virtually all of the approximations listed above. Nevertheless, when the evidence of medium correction (density-dependence) effects upon the

two-nucleon  $t$  matrices as delineated by studies of ( $p, p'$ ) reactions are also considered, it is evident that considerable care should be taken about the proper  $t$  matrices and, consequentially, of a pertinent reaction theory in which to use them.<sup>8</sup> Thus use of the Love-Franey (LF)  $t$  matrices,<sup>9</sup> as most of the ( $p, n$ ) studies have done, give cause for concern. Those complex, energy-dependent  $t$  matrices were constrained to fit two-nucleon phase shifts but designed for use in the distorted-wave impulse approximation (DWIA) analyses of ( $p, p'$ ) and ( $p, n$ ) data. Hence, only their on-the-energy-shell properties have relevance and medium corrections are not encompassed, although recently<sup>4</sup> there has been an attempt to treat those effects on the average. Furthermore, a very recent study<sup>10</sup> has stressed that the nonunitary nature of the LF  $t$  matrices abrogates a proper underlying basis to believe in their operator structure and form.

Medium corrections to the free-two-nucleon  $t$  matrix have been studied by a number of authors.<sup>11-13</sup> For projectile energies of 120 MeV and above, the primary cause of medium corrections is that of Pauli blocking whereby the kernel of the Lipmann-Schwinger equation is varied from the free-scattering case<sup>14</sup> by the constraint of a Fermi sea. Allowance may also be made for central field effects by using an effective-mass approximation in the propagator. The results are distinctive variations from the free-particle case in both on- and off-of-the-energy-shell properties of the two-nucleon  $t$  matrix. But to use any microscopic interaction in the standard distorted-wave approximation (DWA) computer code<sup>15</sup> (a modified form of DWBA70), it is necessary to map the exact  $t$  matrices onto a complex, energy-dependent, and local coordinate space interaction form. This interaction comprises central, tensor, and two-body spin-orbit components each of which has form factors of linear combinations of Yukawa functions of fixed range. The strength of these functions is complex and energy dependent, and varies with Fermi momenta, or equivalently, density. Tabulations have been prepared<sup>12</sup> that are based upon the Paris two-nucleon potential.<sup>16</sup>

A number of studies have demonstrated that the Hamburg  $t$  matrices are appropriate for use in nuclear reaction analyses. They have been folded with various ground-state density profiles to determine microscopic

optical-model potentials<sup>13</sup> that have led to good fits to elastic proton scattering data. They have also been used in analyses of inelastic proton scattering data, again providing fits to data when appropriate transition densities have been available.<sup>17,18</sup> Furthermore, characteristic momentum-transfer signatures of the density dependence were found in those analyses of data. But by and large those tests were of natural parity excitations for which the tensor force does not contribute significantly. For transitions that have large contributions from the isovector tensor force, in particular, there are some suggestions<sup>19</sup> that in this component, the Hamburg  $t$  matrix is too weak. This point will be raised by the analyses we report herein.

Given that inelastic and charge-exchange reactions initiated with (intermediate energy) protons need be analyzed at the very least using fully antisymmetrized, DWA calculations with complex energy- and density-dependent  $t$  matrices, then we must also specify the nuclear transition density matrices for which models of nuclear spectroscopy are required. For light nuclei, the  $0p$  shell model is the standard against which all comparisons are made. Of such models, those designated<sup>20</sup> as 8-16 POT and 2 BME, from which the transition densities as listed by Lee and Kurath<sup>21</sup> were obtained, are the most commonly used. Of course, better models of spectroscopy in the form of wave functions generated in a larger basis space and/or of core-polarization corrections will alter such transition density matrix elements, not only varying the  $0p$  shell values from those of the standard models but also by defining new matrix elements altogether.

How large the corrections are to the standard  $0p$  shell model nuclear transition density matrices is both nucleus and state dependent. However, some general studies of core-polarization effects<sup>22,23</sup> have shown that the corrections, reflecting multi- $h\omega$  components in the real wave functions, enhanced transition strengths of isoscalar electric multipole character while magnetic moments and transition strengths usually are quenched. In developing such corrections the tensor force plays a significant role and calculations must be made to second order at the very least, since a recent study<sup>24</sup> of magnetic moments of  $^{15}\text{N}$  and  $^{17}\text{O}$  found that second-order core-polarization contributions were as large as those of meson exchange current contributions. Therein<sup>24</sup> it was observed that the corrections tend to cancel, leaving the nuclear properties near single-particle and single-hole values. That need not be the case for other properties of the light nuclei and as noted by Towner and Khanna<sup>23</sup> "it would be useful if some of these experiments [( $ee'$ ), ( $pp'$ ), ( $pn$ )] could be completed on odd mass nuclei of closed shell plus one configuration and the  $M1$  component of the spin-flip transition (density) identified. Then some of the calculations (on  $M1$  quenching) could be more qualitatively tested." Hence our interest in  $^{13}\text{C}$ , and specifically in the properties, static and dynamic, of the ground ( $\frac{1}{2}^+ - \frac{1}{2}^+$ ), 3.68 MeV and ( $\frac{3}{2}^- - \frac{3}{2}^-$ ) 15.11 MeV states and their analogs in  $^{13}\text{N}$ .

Besides the magnetic moment,  $\beta$ - and  $\gamma$ -decay properties of  $^{13}\text{C}$  ( $^{13}\text{N}$ ) very good electron scattering data has been measured.<sup>25</sup> Also, at intermediate energies, both

proton inelastic and charge-exchange cross sections have been obtained to complement the pion inelastic scattering measured values that were used to test a basic nuclear structure model.<sup>21</sup> That same basic  $0p$  shell model was modified<sup>26</sup> to include  $2h\omega$  admixtures and then used<sup>27</sup> to study the  $\gamma$ -ray transition properties of  $^{13}\text{C}$ . Essentially this model enhanced the  $C2$  matrix elements above those given by the basic  $0p$  shell model leaving the  $M1$  matrix elements affected little. But electron scattering (transverse) form factors cannot be fit without reduction of the  $M1$  elements. In a study of first-order core-polarization corrections<sup>22</sup> due to the tensor force dominantly, further multi- $h\omega$  corrections to the  $0p$  shell models of spectroscopy enabled a fit to the (ground-state) transverse form factor to  $2\text{ fm}^{-1}$  momentum transfer. No current model of structure (or corrections to transition operators) can explain the very large values for that form factor at even higher-momentum-transfer values,<sup>25</sup> however.

Other views about the electromagnetic properties of nuclei, and of  $^{13}\text{C}$  in particular, exist. One of these<sup>28</sup> supposes that variation of nuclear structure details within the  $0p$  shell suffices to explain data. By making adjustments to the basic  $0p$  shell-model wave functions, Singham<sup>28</sup> was able to fit a range of data. But this view is not favored as it also supposes that transition operators themselves are not affected and so are unchanged from the free-nucleon specifications. A second view was taken by Cheon<sup>29</sup> who used the Cohen and Kurath spectroscopic model but adjusted the nucleon form factor to obtain transverse electron scattering form factors in agreement with data.

Clearly additional and complementary data are required to select amongst the various options and possibilities for the spectroscopy of  $^{13}\text{C}$  ( $^{13}\text{N}$ ) in particular, and ( $p, p'$ ) and ( $p, n$ ) scattering initiated by protons of intermediate energy are good candidates. Likewise, it is clear this additional data must be analyzed using a completely antisymmetrized, DWA method with medium corrected, two-nucleon  $t$  matrices. Such we report herein, and specifically we shall use the 135 MeV ( $p, p'$ ) data of Collins *et al.*,<sup>18</sup> the 160 MeV ( $\bar{p}, n$ ) data reported in the paper of Rappaport *et al.*,<sup>5</sup> and 200, 300, and 400 MeV ( $p, n$ ) data that have been provided for use prior to their publication by the TRIUMF collaboration of Alford *et al.*<sup>1</sup> The latter data, hereafter will be referred to as the TRIUMF data.

## II. SPECTROSCOPIC AMPLITUDES AND TRANSITION PROBABILITIES

The nuclear structure information relevant for calculating transitions between nuclear states caused by one-body processes is embodied in particle-hole matrix elements (one-body density-matrix elements)

$$d_{j_1 j_2}^{(\alpha_1 \alpha_2)} = \langle \Psi_{M_f T_f}^{J_f} | a_{m_2 \alpha_2}^{j_2 \dagger} a_{m_1 \alpha_1}^{j_1} | \Psi_{M_i T_i}^{J_i} \rangle, \quad (1)$$

in which the nucleon creation (annihilation) operators are in the  $j$ - $j$  representation with  $\alpha$  being  $\frac{1}{2}$  for a neutron and  $-\frac{1}{2}$  for a proton.

It is convenient to expand the product of operators in a coupled form such as

$$a_{m_2\alpha_2}^{j_2^\dagger} a_{m_1\alpha_1}^{j_1} = \sum_{IM} (-)^{j_1 - m_1} \langle j_2 j_1 m_2 - m_1 | IM \rangle (a_{\alpha_2}^{j_2^\dagger} \times \bar{a}_{\alpha_1}^{j_1})_M^I, \quad (2)$$

wherein  $\bar{a}_{-m_1\alpha_1}^{j_1}$  identifies  $(-)^{j_1 - m_1} a_{m_1\alpha_1}^{j_1}$ , so that the entity in the square brackets is the  $M$ th component of an irreducible tensor operator of rank  $I$ . One can also couple in isospin space giving

$$a_{m_2\alpha_2}^{j_2^\dagger} a_{m_1\alpha_1}^{j_1} = \sum_{IM\tau\rho} (-)^{j_1 - m_1} (-)^{1/2 - \alpha_1} \langle j_2 j_1 m_2 - m_1 | IM \rangle \langle \frac{1}{2} \frac{1}{2} \alpha_2 - \alpha_1 | \tau\rho \rangle (a^{j_2^\dagger} \times h^{j_1})_{M\rho}^I, \quad (3)$$

with the hole creation operator defined by

$$h_{-m_1 - \alpha_1}^{j_1^\dagger} = (-)^{j_1 - m_1} (-)^{1/2 - \alpha_1} a_{m_1\alpha_1}^{j_1}.$$

With the help of the Wigner-Eckart theorem we can then recast the one-body density-matrix element as

$$d_{j_1 j_2}^{(\alpha_1 \alpha_2)} = \sum_{IM} (-)^{j_1 - m_1} \langle j_2 j_1 m_2 - m_1 | IM \rangle \langle J_i I M_i M | J_f M_f \rangle S_{j_1 j_2 I}^{(\alpha_1 \alpha_2)} / (\hat{J}_f)^{1/2}. \quad (4)$$

We use the notation  $\hat{a}$  to represent  $(2a + 1)$ . The spectroscopic amplitudes in Eq. (4) are the singly reduced matrix elements (in Racah's definition)

$$S_{j_1 j_2 I}^{(\alpha_1 \alpha_2)} = \langle \Psi_{P_f}^{J_f T_f} \| (a_{\alpha_2}^{j_2^\dagger} \times \bar{a}_{\alpha_1}^{j_1})^I \| \Psi_{P_i}^{J_i T_i} \rangle. \quad (5)$$

For inelastic scattering excitations, it is sufficient to use the results of Eq. (5) since the isospin values are constrained by

$$P_i = P_f = T_i,$$

$$\alpha_1 = \alpha_2 = \alpha.$$

But it is often helpful to use spectroscopic amplitudes deduced from an isospin coupled form, which, for inelastic scattering, we identify by

$$\begin{aligned} S_{j_1 j_2 I}^{(\alpha\alpha)} &= \sum_{\tau} (-)^{1/2 - \alpha} \langle \frac{1}{2} \frac{1}{2} \alpha - \alpha | \tau 0 \rangle \langle \Psi_{T_i}^{J_f T_f} \| (a_{\alpha}^{j_2^\dagger} \times h_{\alpha}^{j_1})_0^I \| \Psi_{T_i}^{J_i T_i} \rangle \\ &= (2)^{-1/2} \sum_{\tau} (-)^{(1/2 - \alpha)\tau} S_{j_1 j_2 I}^{(\tau)}, \end{aligned} \quad (6)$$

so that the isospin coupled amplitudes are defined as the reduced matrix elements in Eq. (6).

For charge-exchange ( $p, n$ ) reactions  $\alpha_1$  must be  $\frac{1}{2}$  and  $\alpha_2$  must be  $-\frac{1}{2}$  so that the spectroscopic amplitude becomes

$$\begin{aligned} S_{j_1 j_2 I}^{(1/2 - 1/2)} &= \langle \Psi_{(T_i - 1)}^{J_f T_f} \| (a_{-1/2}^{j_2^\dagger} \times \bar{a}_{1/2}^{j_1})^I \| \Psi_{T_i}^{J_i T_i} \rangle \\ &\equiv \left[ \frac{\langle T_i 1 T_i - 1 | T_f T_i - 1 \rangle}{\langle T_i 1 T_3 0 | T_f T_3 \rangle} \right] S_{j_1 j_2 I}^{(\tau=1)}. \end{aligned} \quad (7)$$

For the target of  $^{13}\text{C}$ ,  $T_i = \frac{1}{2} = T_3$  and so the Clebsch-Gordan coefficient ratio is  $(2)^{1/2}$  for final ( $^{13}\text{N}$ ) states with  $T_f$  of  $\frac{1}{2}$ , and  $(2)^{-1/2}$  for the  $T_f = \frac{3}{2}$  cases. The squared ratio is relevant in relating the cross-section value of ( $p, n$ ) and ( $p, p'$ ) reactions to isobaric analogue states.

When the structure calculations involve only the  $0p$  shell, it is particularly informative to express the spectroscopic amplitudes in the ( $LS$ ) representation, viz.

$$S_{I(LS)}^{(\alpha_1 \alpha_2)} = \sum_{j_1 j_2} (\hat{j}_1 \hat{j}_2 \hat{L} \hat{S})^{1/2} \begin{bmatrix} 1 & 1 & L \\ \frac{1}{2} & \frac{1}{2} & S \\ j_2 & j_1 & I \end{bmatrix} S_{j_1 j_2 I}^{(\alpha_1 \alpha_2)}. \quad (8)$$

In this representation, the amplitudes for inelastic scattering scale those tabulated by Lee and Kurath<sup>21</sup> (LK) as

$$S_{I(LS)}^{(\alpha\alpha)} = (\hat{J}_f)^{1/2} A_{I(LS)\alpha}. \quad (9)$$

Calculations (and results therefrom) obtained by using these spectroscopic amplitudes will be identified hereafter as LK.

When the  $0p$  radial wave functions are chosen to be independent of the  $j$  value, the  $I(LS)$  amplitudes are direct measures of orbital and spin transition probabilities. Then, as transitions are frequently dominated by a single multipole contribution in a particular region of momentum-transfer values, analysis of a composite set of data such as  $\gamma$ - and  $\beta$ -decay probabilities, electron scattering form factors and inelastic scattering via hadronic interactions could provide comprehensive and complementary tests of those amplitudes. Of these, the  $\gamma$ - and  $\beta$ -decay probabilities are essentially zero-momentum-transfer properties and it is convenient to incorporate an analysis of such data herein with the specifications of spectroscopic amplitudes. The use of those amplitudes in analyses of the form factors, etc., from electron and hadron scattering (finite-momentum-transfer attributes) will be discussed subsequently. The

recent observation<sup>38</sup> of binding-energy effects will also be discussed.

In addition to the LK model, two other models of spectroscopy for <sup>13</sup>C have been used in our studies. The first is proposed by Singham<sup>28</sup> in which properties of the ( $\frac{1}{2}$ - $\frac{1}{2}$ ) ground state and ( $\frac{3}{2}$ - $\frac{3}{2}$ ) state at 15.11 MeV excitation in <sup>13</sup>C were fitted to determine wave functions constrained within the 0p shell. The second model of spectroscopy of <sup>13</sup>C (<sup>13</sup>N) is based upon calculations of Millener<sup>26</sup> wherein  $2h\omega$  excitations were included in the description of the  $T = \frac{1}{2}$  states.

These three models of structure have slightly different orbit occupation numbers for the ground state. Those values are shown in Table I. Compared to the LK case, both of the other models have an increased  $0p_{1/2}$  shell occupancy with a decrease in the  $0p_{3/2}$  shell occupancy, especially for protons. Aside from the small occupancies of higher orbitals, there is a fair degree of similarity between the shell occupation values of the Millener and Singham models.

In all cases the dominant transition components are within the 0p shell whence data are most easily discussed using the  $I(LS)$  representation. Hence for the 0p shell transitions, the isoscalar ( $\tau=0$ ) and isovector ( $\tau=1$ ) spectroscopic amplitudes,  $S_{I(LS)}^{(\tau)}$ , are listed in Table II for the ( $\frac{1}{2}$ - $\frac{1}{2}$ ) ground state of <sup>13</sup>C. The amplitudes for the other two states of interest at 3.68 and 15.11 MeV, respectively, are contained in Tables IV and VII to be discussed later.

We note that the 0p contributions in the Millener spectroscopic model arise not solely from the  $(0s)^4(0p)^9$  configuration but also from other allowed components in the wave functions. The effects of  $(1s-0d)$  and  $(1p-0f)$  shell nucleons will be stressed in our discussions of each state. But before doing so, it is useful to note some observation and general conditions pertinent to nuclei in the

mass region.

Wilkinson<sup>30</sup> analyzed 20 strong Gamow-Teller  $\beta$ -decay transitions within the 0p shell and the lower-mass ( $1s-0d$ ) shell nuclei. He concluded that shell-model transition probabilities were generally stronger than observed, leading to an empirical suppression factor of  $0.90 \pm 0.03$  for the transition matrix element. Recent  $(p, n)$  experiments have been interpreted as requiring stronger suppression. We will discuss this effect as a suppression factor  $G_1$  for the isovector spectroscopic amplitude  $S_{1(01)}^{(1)}$ .

One does not expect the same suppression for isovector  $M1$  transitions as for Gamow-Teller decays, since meson exchange contributions are generally larger for the  $M1$  case. However, there do not seem to be large differences in our cases, so we use a single  $G_1$  factor.

It is well known that  $C2$  transitions calculated in the 0p shell space are sometimes too weak when compared with observation. For example, the (isoscalar)  $B(C2)$  between the ground and first excited  $2^+$  state at 4.44 MeV in <sup>12</sup>C is calculated to be but  $\frac{1}{2}$  of the measured value. This is known to be due to the inadequacy of the 0p space for representing quadrupole deformation. But one can account for that by using an enhancement factor,  $E_0$ , for the isoscalar spectroscopic amplitude,  $S_{2(20)}^{(0)}$ . We note that such an enhancement is needed essentially for transitions between states that may be considered to be members of a rotational band. Such is the case for the transition to the ( $\frac{3}{2}$ - $\frac{1}{2}$ ) state at 3.68 MeV in <sup>13</sup>C from the ( $\frac{1}{2}$ - $\frac{1}{2}$ ) ground state.

#### A. The ( $\frac{1}{2}$ - $\frac{1}{2}$ ) ground state

Since the magnetic moments of both <sup>13</sup>C and <sup>13</sup>N are known to three-figure accuracy we can consider their sum and difference to compare with the isoscalar and isovector properties of the three models of spectroscopy via

$$\frac{1}{2}[\mu(^{13}\text{C}) + (-)^\tau \mu(^{13}\text{N})] = (6)^{-1/2} \{ (3)^{1/2} [\mu_\nu + (-)^\tau \mu_\pi] S_{1(01)}^{(\tau)} + (2)^{1/2} (-)^\tau S_{1(10)}^{(\tau)} \}, \quad (10)$$

in which  $\mu_\nu$  ( $\mu_\pi$ ) are the neutron (proton) magnetic moment of  $-1.913$  ( $2.793$ ) nm. With the spectroscopic amplitudes listed in Table II, the numerical results for the isoscalar and isovector mass 13 moments are as listed in Table III. The last column in this table gives the Gamow-Teller strengths, which are defined by the gen-

eral transition formula

$$B_{\text{GT}}(i \rightarrow f) = (\hat{J}_i)^{-1} 6R^2 |S_{1(01)}^{(1)}|^2, \quad (11)$$

wherein  $R$  is the Clebsch-Gordan coefficients ratio for the <sup>13</sup>C case

TABLE I. Ground-state occupancies for <sup>13</sup>C.

Orbit	Protons			Neutrons		
	LK	Singham	Millener	LK	Singham	Millener
$0s_{1/2}$	2	2	1.992	2	2	1.996
$0p_{3/2}$	3.520	3.093	3.215	3.868	3.801	3.692
$0p_{1/2}$	0.480	0.907	0.706	1.132	1.199	1.185
$1s-0d$			0.080			0.096
$1p-0f$			0.007			0.031

TABLE II. The amplitudes  $S_{1(LS)}^{(\tau)}$  from  $0p$  contributions to the  $(\frac{1}{2}^{\pm}\frac{1}{2})$  ground state.

$I(L,S)$	Isoscalar ( $\tau=0$ )			Isovector ( $\tau=1$ )		
	LK	Singham	Millener	LK	Singham	Millener
1(2,1)	0.968	0.989	0.858	0.890	0.715	0.768
1(0,1)	-0.238	-0.223	-0.220	-0.232	-0.195	-0.230
1(1,0)	0.579	0.569	0.556	0.348	0.237	0.215

$$R = \langle T_i 1 T_3 \pm 1 | T_f T_3 \pm 1 \rangle / \langle T_i 1 \frac{1}{2} 0 | T_f \frac{1}{2} \rangle .$$

The experimental value of  $B_{GT}({}^{13}\text{N})$  was extracted from the measured  $ft$  values via

$$B_F + (g_A/g_V)^2 B_{GT} \equiv 6166/ft , \quad (12)$$

wherein with  $B_F$  taken as 1 we have used the value<sup>31</sup> of  $1.260 \pm 0.007$  for the ratio  $(g_A/g_V)$ . In his analysis<sup>28</sup> Singham has used different beta constants in Eq. (12) to extract the empirical value of  $B_{GT}({}^{13}\text{N})$  for use in his fitting process. The  $B_{GT}$  values given by the LK and Millener spectroscopic models are clearly too large as is also the case for the moment difference. Even applying a suppression factor  $G_1$  to the isovector spin amplitude cannot bring the LK result close to both the moment difference and  $B_{GT}$  values. However this is possible with the Millener amplitudes with a value  $G_1$  of 0.82. The reason is that the orbital contribution [amplitude with  $I(LS)$  of 1(1,0)] to the moment difference is much less in

the enlarged space and so the simultaneous fit is possible. The contributions from nucleons in the  $(1s-0d)$  and  $(1p-0f)$  levels are small but not negligible, and as a result the moment difference and  $B_{GT}$  values increase slightly. However, a suppression factor of 0.79 gives results close to those listed in the second to last line of Table III.

### B. The $(\frac{3}{2}^{\pm}\frac{1}{2})$ state at 3.68 MeV

The spectroscopic amplitudes for  $0p$  shell-model transitions to the  $(\frac{3}{2}^{\pm}\frac{1}{2}; 3.68 \text{ MeV})$  state in  ${}^{13}\text{C}$  are given in Table IV, with which the  $\gamma$ -decay rates given in Tables V and VI were evaluated.

This state decays by  $M1$  and  $C2$   $\gamma$  rays to the ground state in  ${}^{13}\text{C}$  with an  $M1$  component involving  $(LS)$  transition operators associated with the 1(10) and 1(01) amplitudes. Specifically,

$$(\hat{J}_i)B(M1; i \rightarrow f) = \left(\frac{3}{4}\pi\right) \left\{ \sum_{\tau} (3)^{1/2} [\mu_{\nu} + (-)^{\tau} \mu_{\pi}] S_{1(01)}^{(\tau)} + (2)^{1/2} (-1)^{(\tau)} S_{1(10)}^{(\tau)} \right\}^2 , \quad (13)$$

with the expression on the right-hand side being the square of the sum of reduced matrix elements (RME). [Bare values of the nucleon moments are often replaced with effective values to account for the limited basis of the model of spectroscopy. Herein, we use the  $LS$  representation of transition density matrix elements and so instead consider scale factors (such as  $G_1, E_0$ ) upon the spectroscopic amplitudes to encompass core-polarization effects.] Using the LK and Millener model spectroscopic amplitudes we obtain the RME's  $B(M1)$  values and the Gamow-Teller  $\beta$ -decay strengths,  $B_{GT}$ , that are listed in

Table V. The  $B_{GT}$  values were calculated using Eq. (11), but as there is no  $\beta$  decay to the  $(\frac{3}{2}^{\pm}\frac{1}{2})$  state in  ${}^{13}\text{C}$ , the experimental value must be inferred from the  $(p,n)$  cross section. This will be discussed later.

By using the same suppression factor  $G_1$  of 0.82 as with the ground-state case, the calculated  $B(M1)$  obtained with the  $0p$  shell components of the Millener spectroscopy is in reasonable agreement with the observed value. The corresponding (suppressed) value of  $B_{GT}$  is given in the last column of Table V. Inclusion of all of the  $2h\omega$  admixtures from the Millener calculation gives

TABLE III. Magnetic moments of mass 13 and  $B_{GT}({}^{13}\text{N})$ .

	$\frac{1}{2}[\mu({}^{13}\text{C}) + \mu({}^{13}\text{N})]$	$\frac{1}{2}[\mu({}^{13}\text{C}) - \mu({}^{13}\text{N})]$ (spin + orbital)	$B_{GT}({}^{13}\text{N})$
LK	0.186	0.772 - 0.201 = 0.571	0.323
Singham	0.190	0.649 - 0.137 = 0.512	0.228
Millener	0.184	0.765 - 0.124 = 0.641	0.317
Millener ( $G_1=0.82$ )	0.184	0.503	0.213
Expt. <sup>a</sup>	$0.190\mu_N$	$0.512\mu_N$	$0.206 \pm 0.003$

<sup>a</sup>Data as reported in Ref. 39.

TABLE IV. The spectroscopic amplitudes,  $S_{I(LS)}^{(\tau)}$ , for the  $0p$  shell contribution to excitations of the  $(\frac{3}{2}^{-}\frac{1}{2}^{-}; 3.68 \text{ MeV})$  state in  $^{13}\text{C}$ .

$I(LS)$	Isoscalar ( $\tau=0$ )		Isovector ( $\tau=1$ )	
	LK	Millener	LK	Millener
1(2,1)	-0.266	-0.244	-0.294	-0.257
1(1,1)	-0.440	-0.439	-0.454	-0.348
1(0,1)	-0.581	-0.602	-0.629	-0.599
1(1,0)	0.355	0.375	0.171	0.066
2(2,1)	1.038	0.869	0.523	0.561
2(1,1)	0.723	0.535	0.016	0.092
2(2,0)	-1.505	-1.488	0.274	0.307

somewhat larger values, but values for which a suppression factor of 0.79 will yield results close to those given in the second to last line of Table V.

The  $C2$  transition involves the  $I(LS)=2(20)$  proton amplitudes and, in the isospin notation we obtain

$$(\hat{J}_i)B(C2; i \rightarrow f) = (15e^2b^4/8\pi)[S_{2(20)}^{(0)} - S_{2(20)}^{(1)}]^2, \quad (14)$$

wherein the right-hand side is again the square of a reduced matrix element. With an oscillator length  $b$  of 1.64 fm those RME's and the  $B(C2)$  for excitation of this  $\frac{3}{2}^{-}\frac{1}{2}^{-}$  state as calculated by the various spectroscopic models are listed in Table VI. The  $0p$  shell-model results are about 50% of the measured values and the  $2h\omega$  additions to complete the Millener model of spectroscopy give a substantial increase but still not enough to yield the observed value. With the LK structure model an enhancement factor,  $E_0$ , of 1.46 gives a match to the data. [Effective charges for proton and neutrons are frequently used with limited basis space models of spectroscopy. As with the  $B(M1)$  study, however, we find it convenient to use scale factors relevant to the  $LS$  representation spectroscopic amplitudes to making a match to data values.] That enhancement is essentially the same needed to match the LK,  $0p$  shell model, estimate to the measured  $B(C2)$  value for the excitation of the  $2_1^+$  state in  $^{12}\text{C}$ .

Our analyses of the larger basis Millener spectroscopy

TABLE V. The  $B(M1)$  and  $B_{GT}$  values for the excitation of the  $(\frac{3}{2}^{-}\frac{1}{2}^{-}; 3.68 \text{ MeV})$  state from the ground state in  $^{13}\text{C}$ .

	RME <sup>a</sup> ( $\tau=0$ )	RME ( $\tau=1$ ) <sup>a</sup> (spin + orbital)	$B(M1)$ ( $\mu_N$ ) <sup>2</sup>	$B_{GT}$
LK	-0.187	(2.505-0.118)=2.387	2.42	2.37
Millener	-0.189	(2.386-0.046)=2.340	2.31	2.15
Millener ( $G_1=0.82$ )			1.48	1.45
Expt. <sup>b</sup>			1.39±0.14	

<sup>a</sup>Reduced matrix element values computed using select isospin components of Eq. (13).

<sup>b</sup>Data as reported in Ref. 39.

TABLE VI. The  $B(E2)$  values for the excitation of the  $(\frac{3}{2}^{-}\frac{1}{2}^{-})$  state at 3.68 MeV in  $^{13}\text{C}$ . (Units are  $e^2\text{fm}^4$ .)

	RME <sup>a</sup> ( $\tau=0$ )	RME <sup>a</sup> ( $\tau=1$ )	$B(E2)$
LK	3.127	0.569	6.83
Millener	3.092	0.638	6.96
Millener (total)	3.962	0.557	10.21
LK ( $E_0=1.46$ )	4.565	0.569	13.18
Expt.			13.2±1.4 <sup>b</sup>

<sup>a</sup>Reduced matrix elements computed using select isospin elements in Eq. (14).

<sup>b</sup>Data as reported in Ref. 39.

values revealed the major cause of the increase from a prediction of 6.96 to 10.21  $e^2\text{fm}^4$  to be transitions between the  $0s(0p)$  and  $0d(0f)$  shells. Such is a reflection of quadrupole deformation of the mean field in going beyond the  $(0s)^4(0p)^9$  space. An enhancement factor of 1.16 ( $E_0$ ) is still required to agree with the observed value of 13.2  $e^2\text{fm}^4$ .

### C. The $(\frac{3}{2}^{-}\frac{3}{2}^{-})$ state at 15.11 MeV

Spectroscopic amplitudes for the excitation, from the ground, of this lowest  $T=\frac{3}{2}$  state in  $^{13}\text{C}$  have been calculated only within the  $(0s)^4(0p)^9$  model space. The values for this isovector excitation have been obtained from both the LK and Singham spectroscopic models and are listed in Table VII. The Singham and LK amplitudes differ most noticeably for the  $I(L,S)$  combinations of 1(10), 2(2,1), and 2(1,1), with Singham's values all being smaller.

From these spectroscopic amplitudes, by using Eq. (11)–(14) the  $\beta$  decay of the analogue state in  $^{13}\text{B}$  and the isovector  $M1$  and  $C2$  ( $\gamma$ -ray) excitations from the  $^{13}\text{C}$  ground state may be evaluated. Their numerical values for both the LK and Singham cases are presented in Table VIII. Of these, the  $B(C2)$  values are larger than experiment but lie within the experimental uncertainty. Therefore, one would not expect enhancement of this isovector  $C2$  amplitude. But we note that the reduced transition rate was extracted from low- $q$  ( $e, e'$ ) data<sup>32</sup> by

TABLE VII. Spectroscopic amplitudes for the excitation of the  $(\frac{3}{2}^{-}\frac{3}{2}^{-})$  state at 15.11 MeV in  $^{13}\text{C}$  ( $0p$  shell contributions).

$I(L,S)$	LK	Singham
1(2,1)	0.274	0.291
1(1,1)	1.140	1.024
1(0,1)	0.458	0.424
1(1,0)	-0.285	-0.150
2(2,1)	-1.030	-0.778
2(1,1)	-0.698	-0.535
2(2,0)	0.995	0.962

TABLE VIII. The  $B(M1)$  and  $B(E2)$  values for the excitation of ( $\frac{3}{2}^--\frac{3}{2}$ ) state at 15.11 MeV  $^{13}\text{C}$  and the  $B_{\text{GT}}(^{13}\text{B})$  for the decay of its analogue state.

	Isovector RME <sup>a</sup> (spin + orbital)	$B(M1)$ ( $\mu_N$ ) <sup>2</sup>	$B(E2)$ $e^2\text{fm}^4$	$B_{\text{GT}}(^{13}\text{B})$
LK	(-1.824+0.197)=-1.627	1.32	2.14	0.472
Singham	(-1.689+0.104)=-1.585	1.26	2.00	0.404
LK ( $G_1=0.9$ )		1.04		0.382
Expt <sup>b</sup>		1.12±0.08	1.9±0.3	0.38±0.01

<sup>a</sup>Reduced matrix elements computed using the isovector components in Eqs. (13) and (14).

<sup>b</sup>Data as reported in Ref. 39.

fitting a straight line through three data points. In this case they do not form a very good straight line. Also, a study of mirror  $\gamma$  decays<sup>40</sup> gave the ( $^{13}\text{N}$ ) C2 width about one-half of the ( $^{13}\text{C}$ ) value of Wittwer *et al.*<sup>32</sup> For the LK case, both the  $B(M1)$  and  $B_{\text{GT}}(^{13}\text{B})$  predictions must be quenched to reproduce the measured values, and, specifically the amplitudes must be suppressed with  $G_1$  being 0.9, a value in agreement with the general result found by Wilkinson<sup>30</sup> but larger than required by similar properties of the ground and  $\frac{3}{2}^--\frac{1}{2}$  states.

### III. FINITE-MOMENTUM-TRANSFER DATA AND ANALYSES

The  $^{13}\text{C}$  states of interest, and their analogues in  $^{13}\text{N}$ , have been studied via electron<sup>25,32,33,38</sup> and proton scattering,<sup>18</sup> and by charge-exchange ( $p,n$ ) reactions to the analogue states.<sup>5,6</sup>

From electron scattering, longitudinal and transverse form factors have been extracted to be compared with calculations based upon

$$|F^{(x)}(q)|^2 = [4\pi/(Z^2\hat{J}_i\hat{T})] \left[ \sum_{\alpha j_1 j_2} S_{j_1 j_2 I}^{(\alpha\alpha)} \langle \phi_\alpha^{j_2} \| X_I^{(x)}(q) \| \phi_\alpha^{j_1} \rangle \right]^2, \quad (15)$$

wherein  $x$  signifies longitudinal, transverse electric, or transverse magnetic multipole operators for  $X_I^{(x)}(q)$ . The longitudinal (Coulomb) form-factor operators are

$$X_I^{(c)}(q) = e_\alpha j_I(qr) Y_I(\hat{r}),$$

wherein  $e_\alpha$  is the (effective) charge of a nucleon of type  $\alpha$ . The transverse form-factor operators are more complicated expressions also involving (effective)  $g$  factors. Their details are not essential for this presentation but can be readily deduced using the specifications given by Cheon.<sup>29</sup> Indeed the prime purpose of Eq. (15) is simply to stress how spectroscopic amplitudes are involved in the definition of electron scattering form factors. Also, for the  $0p$  shell models of the structure considered we will use sets of  $S_{j_1 j_2 I}^{(\alpha\alpha)}$  that coincide to the separate  $S_{I(LS)}^{(\alpha\alpha)}$ , and so again consider matches to (momentum-transfer-dependent) data with scale factors  $G_1, E_0$ , etc. To complete our notation we shall use  $C2$  and  $E2$  to distinguish longitudinal from transverse electric quadrupole characteristics hereafter.

The proton inelastic scattering and charge-exchange reaction data to be considered have been measured with intermediate energy projectiles (100–400 MeV) for which the distorted-wave approximation should be appropriate.<sup>8</sup> Thus we have analyzed such data using calculations of scattering amplitudes

$$T_{i \rightarrow f} = \sum_{j_1 j_2 \alpha m_1 m_2 M} (-)^{j_1 - m_1} \langle j_2 j_1 m_2 - m_1 | IM \rangle \langle J_i IM_i M | J_f M_f \rangle S_{j_1 j_2 I}^{(\alpha\alpha)} \langle \chi_f^{(-)}(0) \phi_{m_2 \alpha}^{j_2}(1) | t^\alpha(01) | \mathcal{A}_{01} [\chi_1^{(+)}(0) \phi_{m_1 \alpha}^{j_1}(1)] \rangle,$$

wherein  $\chi^{(\pm)}$  are the distorted waves to be determined from an optical-model potential,  $\mathcal{A}_{01}$  antisymmetrizes the (initial) two-nucleon state and  $t(01)$  is the appropriate two-nucleon  $t$  matrix between the proton projectile and struck nucleon of type  $\alpha$ . For intermediate energies this two-nucleon  $t$  matrix will be complex, energy dependent, and nuclear medium influenced.<sup>11</sup> Furthermore, its off-the-energy shell properties are involved in reaction calculations.<sup>8</sup> For energies in excess of about 120 MeV the Pauli blocking effect is the preponderant “many-body” correcting feature in the specification of the  $t$  matrix to distinguish it from the free two-particle  $t$  matrix, whether

that is derived from solution of the Lippmann-Schwinger equation<sup>14</sup> or developed phenomenologically for use in impulse approximation, distorted-wave calculations.<sup>9</sup> The latter of these free  $t$  matrices is the subject of some recent criticism.<sup>10</sup>

Herein we will use the energy- and density-dependent  $t$  matrices that have been developed<sup>12</sup> from solutions of the Bethe-Goldstone equation, starting with the Paris interaction.<sup>16</sup> We designate this as the Hamburg  $t$  matrix hereafter. It has been used most successfully in many analyses of elastic and inelastic proton scattering data.<sup>13,17,18</sup>

With harmonic oscillator ( $b = 1.64$  fm) wave functions representing the bound states, all scattering amplitudes have been calculated using a modified form of the code DWBA70 in which the exact exchange amplitudes are computed and all multipole contributions are summed coherently.

Use of harmonic oscillator radial wave functions, albeit convenient, can be problematic for certain details of data analyses. Recently,<sup>38</sup> the transverse form factors for ( $ee'$ ) on  $^{13}\text{C}$  were shown to be sensitive to the choice of radial functions and for  $M1$  components in particular. Certainly weakly bound single-particle state radial functions, such as those of the  $s$ - $d$  shells for  $^{13}\text{C}$ , could be markedly different from harmonic-oscillator functions. In this paper the case of transitions to the  $\frac{3}{2}^{\pm}\frac{3}{2}$  state is most sensitive to the radial wave functions. This is because the common parentage of the initial and final state is composed of the lowest  $T=1$  states in  $^{12}\text{C}$ . Because of the difference in binding of the states and because the neutron transition densities are the negatives of the corresponding proton transition densities for an isospin-changing transition, the use of Woods-Saxon radial functions could make an appreciable difference. We have not calculated this effect. We have used oscillator functions in the analysis of a wide range of complementary data, seeking from correlations to delineate to what extent one can interpret the observations, assuming the radial overlaps are not a serious problem.

Essentially we start with the  $p$  shell-model suppression (enhancement) factors deduced heretofore from analyses of low- $q$  data and enquire what is required thereafter by better analyses of data and/or by analyses of data taken at larger momentum-transfer values.

#### A. The $\frac{1}{2}^{\pm}\frac{1}{2}$ (ground) state

The  $M1$  (elastic) electron scattering form factor and charge-exchange ( $p, n$ ) scattering to the ground state of  $^{13}\text{N}$  are considered herein. In these analyses, all of the  $M1$  spectroscopic amplitudes of Table II give significant contributions. But for all models the predominant amplitude is that of a neutron rearrangement in the  $0p_{1/2}$  orbit. The LK amplitude  $S_{1/2,1/2}^{(1/2,1/2)}$  has a value of 1.505 for example, and the Singham model value of this amplitude is 1.36. Other  $j$ - $j$  coupling amplitudes are important but have magnitudes of the order 0.15 at best.

The magnetic dipole form factor (transverse) from elastic scattering of electrons has been measured<sup>25</sup> to momentum-transfer values of  $4\text{ fm}^{-1}$ . That form factor for  $q > 2\text{ fm}^{-1}$  is quite unusual in that the observed data far exceeds all calculated values and indeed by so much that no standard shell-model wave function even corrected for core-polarization, meson exchange currents, or effective operator scales can hope to explain the magnitudes in the vicinity of  $3.5\text{ fm}^{-1}$ . We limit our consideration therefore to the region  $0$ – $2\text{ fm}^{-1}$  in momentum transfer. The complete data, nevertheless, are presented in Fig. 1 in comparison with the results from our calculations of the elastic  $M1$  form factor obtained using the Millener and LK models of the structure as indicated. On the left-hand side in this figure, the isoscalar ( $T=0$ ),

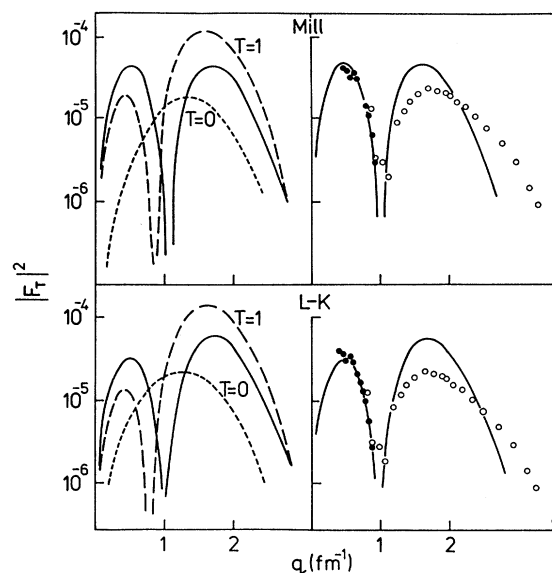


FIG. 1. The elastic scattering (electron) magnetic form factor from  $^{13}\text{C}$ . The isoscalar ( $T=0$ ), isovector ( $T=1$ ), and summed isospin transfer form-factor results are depicted by the short-dashed, long-dashed, and continuous curves, respectively.

isovector ( $T=1$ ), and summed results are given. For momentum-transfer values below  $0.8\text{ fm}^{-1}$  there is constructive interference between the isovector and isoscalar amplitudes. Near the first maximum, the  $1(0,1)$  isovector contribution is most important. If we apply a suppression,  $G_1$ , of 0.82 to the Millener case as suggested by our earlier discussion, then the first maximum is lowered to be slightly under that of the calculated LK result that is shown in Fig. 1. It still remains in reasonable agreement with observations. But there is severe interference between the matrix elements with  $J(L,S)$  of  $1(0,1)$  and  $1(2,1)$ . So strong is that interference that if the neutron  $1(2,1)$  amplitude is reduced to fit high- $q$  data, the low- $q$  form factor can then be compatible with a value for  $G_1$  of 0.8.

There is destructive interference between the isoscalar and isovector amplitudes for momentum-transfer values above  $1\text{ fm}^{-1}$ . Furthermore, near the second maximum of the form factor ( $q \sim 1.6\text{ fm}^{-1}$ ) it is the  $1(2,1)$  isovector component that is the most important. Thus, relative to the LK calculation, the result of the larger space Millener model calculation is to reduce the second maximum in the form factor appreciably. By doing so, we obtain a result closer to, but not as low as, the observed value. We note that a recent calculation<sup>22</sup> required  $12h\omega$  contributions in a harmonic-oscillator model to obtain a fit to this data ( $1$ – $2\text{ fm}^{-1}$ ).

Direct reaction, charge-exchange ( $\vec{p}, n$ ) scattering from  $^{13}\text{C}$  leading to the ground state of  $^{13}\text{N}$  is particularly useful as such data analyses are complementary to those of the elastic, transverse form factor. The transition density matrix elements are the same, with the ( $\vec{p}, n$ ) reaction being sensitive to solely the isovector transition components.

At 160 MeV, both differential cross section and analyz-

ing power data have been measured<sup>5</sup> and those measured values are shown in Fig. 2. They are compared with the results of DWA calculations made using phenomenological optical-model potentials,<sup>5</sup> and the Hamburg density-dependent  $t$  matrix. The results obtained by using the LK and Millener spectroscopic models are displayed on the left- and right-hand sides of this figure with the  $I=0$  and  $I=1$  component contributions depicted by the dash-dotted and dashed lines, respectively. The small-angle scattering data ( $<17^\circ$ ) cross section and analyzing power, are quite well reproduced by both calculations. This scattering angle range coincides with a momentum-transfer range of  $0-0.8 \text{ fm}^{-1}$ ; in which range both models of spectroscopy gave good fits to the elastic, electron scattering, transverse form factor. At the larger scattering angles,  $q > 1 \text{ fm}^{-1}$ , the calculated differential cross sections are a factor of 2 or more larger than the observed data, with the Millener results not as disparate from data as the LK ones. This is again a reflection of the electron form-factor comparisons.

At higher incident energies the  $t$  matrix should equate more readily to the free two-nucleon  $t$  matrix as medium corrections caused by Pauli exclusion and average fields in the propagator of the defining equations for those  $t$  matrices decrease in significance. Distortions should also be less severe. Data has been taken at 200, 300, and 400 MeV at TRIUMF (Ref. 1) and the results are presented in Fig. 3. Therein they are compared with the  $I=0$  (dot-dashed),  $I=1$  (dashed), and summed angular momentum-transfer (continuous) DWA calculation results obtained using the LK (left), Millener (center), and Singham (right) models of spectroscopy. There are minor

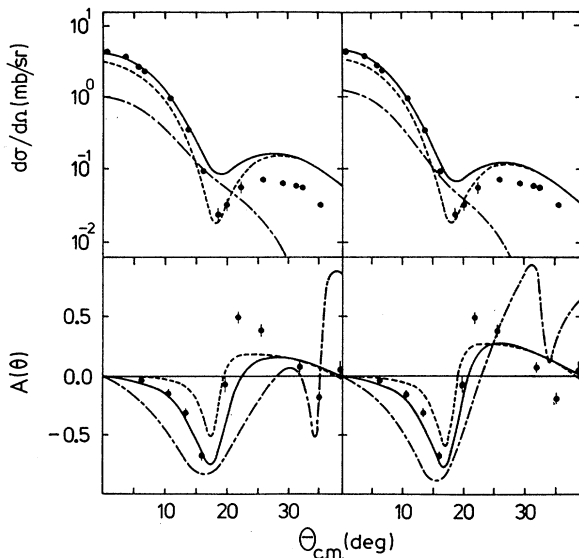


FIG. 2. The differential cross sections (top) and analyzing powers (bottom) from the 160 MeV ( $\bar{p}n$ ) scattering from  $^{13}\text{C}$  and to the ground state of  $^{13}\text{N}$ . The results obtained using the LK and Millener models of spectroscopy are shown on the left- and right-hand side as indicated and with the separate  $I=0$  and  $I=1$  component contributions shown by the dash-dotted and dashed curves, respectively.

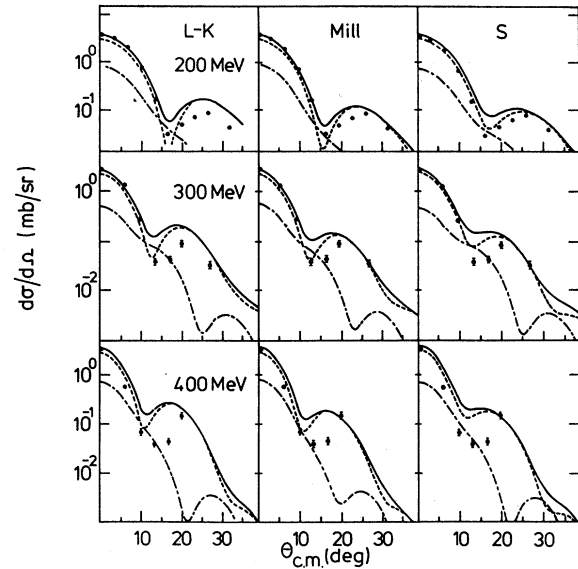


FIG. 3. The results of DWA calculations for the ground-state, charge-exchange ( $p,n$ ) differential cross sections from  $^{13}\text{C}$  and compared with data taken at 200, 300, and 400 MeV incident energy. The calculations were obtained using the LK, Millener, and Singham models of spectroscopy and the separate  $I=0$  and  $I=1$  contributions are depicted by the dash-dotted and dashed curves, respectively.

differences in component contributions and overall transition strength between the results obtained using the different sets of spectroscopic amplitudes with optical-model potentials taken from the literature<sup>34</sup> and the relevant energy, Hamburg  $t$ -matrices. We observe at all energies a good match to the small-angle data with too large predictions at the larger scattering angles.

At all intermediate energies the  $I=1$  transition probabilities dominate the calculated results. There are three  $I(L,S)$  combinations to the spectroscopy used in calculating those  $I=1$  contributions of which only the  $1(0,1)$  and  $1(2,1)$  are significant. The total results for  $I=1$  are shown in Figs. 2 and 3 by the short-dashed curves. At small scattering angles ( $<10^\circ$ ) the "Gamow-Teller,"  $1(0,1)$  component is much larger than that of the  $1(2,1)$  component. The  $I=0$  contributions to these calculations are displayed by the long-dashed curves in Figs. 2 and 3 and they add incoherently to the  $I=1$  values to give the complete result. The  $I=0$  values are due almost entirely to the "Fermi" components for which  $I(L,S)$  is  $0(0,0)$ .

For scattering angles  $<15^\circ$  in the center-of-mass system, the 160 MeV data are well fit by the complete calculation with even the very sensitive, analyzing power data being reproduced. For larger scattering angles, however, that fit is not maintained. In that region the  $1(2,1)$  component becomes large and the interference with the  $1(0,1)$  amplitude severe.

The  $0^\circ$  results of the DWA calculations of 160 MeV ( $\bar{p}$ ) leading to the ground state of  $^{13}\text{N}$  are presented in Table IX. Direct and direct-plus-exchange calculations were made and for all separate  $I(L,S)$  component spectroscopic amplitudes. The differential cross-section

TABLE IX. The  $0^\circ$  calculated values for the 160 MeV  $(\bar{p}, n)$  reaction to the ground state of  $^{13}\text{N}$ .

Component	$d\sigma/d\Omega$ (mb/sr)		Spin-flip probability	
	Direct	Direct + Exchange	Direct	Direct + Exchange
0(0,0)	1.6112	0.9960	0.0	0.0
0(1,1)	0.0001	$< 10^{-4}$	0.0	0.0
$I=0$	1.582	0.996	0.0	0.0
1(0,1)	4.4688	2.8146	0.670	0.673
1(1,0)	$< 10^{-4}$	0.0005	0.601	0.507
1(2,1)	0.0191	0.0209	0.858	0.904
$I=1$	4.686	2.952	0.666	0.617
LK	6.268	3.948	0.498	0.461
Expt. <sup>a</sup>		$4.2 \pm 0.1$		$0.46 \pm 0.2$

<sup>a</sup>Data as given in Ref. 5.

values are compared to the experimental value of  $4.2 \pm 0.1$  whilst the associated spin-flip probability amplitudes are compared with the empirical number of  $0.46 \pm 0.02$ . Clearly, the  $I=0$  and  $I=1$  contributions to the cross section are dominated by the  $I(L, S)$  components 0(0,0) (Fermi) and 1(0,1) (Gamow-Teller), respectively; the latter being almost three times as large as the former.

But it is the crucial role of the exact exchange amplitudes that is stressed by this tabulation. With this inclusion it is clear that both the ‘‘Fermi’’ and ‘‘Gamow-Teller’’ amplitudes for this  $(\bar{p}, n)$  reaction add to and have very good agreement with the cross-section data and maintain their relative contributions so that the calculated value of the analyzing power agrees with experiment. Without these exact amplitudes, and their exact interference with the direct ones, a Gamow-Teller suppression factor  $G_1$  of 0.76 would be touted, so that the  $I=1$  contribution to the cross section would drop from 4.686 to 2.7 mb/sr and the measured  $0^\circ$  value would then fit. By doing so, however, the predicted analyzing power would be changed from 0.498 to 0.41.

In fact, for all three important components [the 1(2,1) contribution increases with scattering angle] and for almost all scattering angles to  $35^\circ$ , the exchange terms interfere destructively with the direct ones. That mix at  $0^\circ$ , however, has given an excellent fit to the ground-state data, and the importance of the exchange amplitudes vitiates use of the data to extract  $\beta$ -decay strengths, other than by using complete DWA analyses of the data.

One of the uncertainties of our analyses is the choice of optical-model potential, with which to specify the distorted waves. However, optical-model potentials have been derived microscopically<sup>35</sup> and using the same  $t$  matrices (Hamburg, density dependent). Using these potentials for 200, 300, and 400 MeV incident energy, the DWA calculations gave results as shown in the left-hand side of Fig. 4 and as identified by the numerals. The results identified as the microscopic optical potential (MOP) and phenomenological optical potential (POP) in that same panel are those for 200 MeV protons and with the microscopic and phenomenological optical-model potentials, respectively. There are noticeable differences of which the most important is the smaller  $0^\circ$  values for the  $(p, n)$  cross section

determined when the microscopic potentials are used; a difference which is consistent with a more diffuse potential. Such variation is sufficient cause for concern about the use of the  $0^\circ$  data and DWA analyses to specify Gamow-Teller and Fermi matrix elements irrespective of the further uncertainties of using the impulse approximations, scaled or partial  $t$  matrices and, in some cases, a simplification to exact exchange amplitudes.

It is interesting to collect all the data as a function of momentum transfer as has been done in the right-hand side of Fig. 4. Clearly there is some variation in the  $0^\circ$  values ( $q \rightarrow 0$  for all data) but to  $0.8 \text{ fm}^{-1}$  the data suggests a well-defined hadronic form factor for this transition. The hatched band gives the spread in calculated values we have obtained using all four energies and all reasonable optical-model potentials in calculations.

Finally, in Fig. 5, the individual  $t$ -matrix component contributions to the DWA calculations of the 200 MeV charge-exchange reaction are displayed. The central force contributions for the dipole ( $I=1$ ), monopole

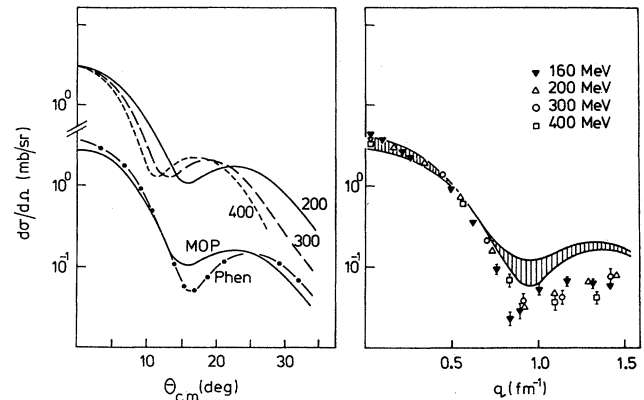


FIG. 4. Left: A comparison of calculated  $(p, n)$  cross sections from the excitation of the ground state of  $^{13}\text{N}$ . Those designated by the incident energies and the label MOP were calculated using microscopic optical-model potentials. Right: All of the  $(p, n)$  data from excitation of the  $^{13}\text{N}$  ground state plotted as a function of the momentum transfer and compared with the calculated results variation with energy and potentials.

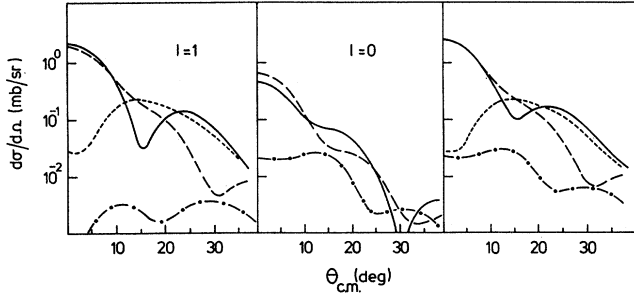


FIG. 5. The individual components of the two-nucleon  $t$  matrix (central, tensor, and two-body spin-orbit) contributions to the  $I=1$ ,  $I=0$ , and summed angular momentum-transfer results from DWA calculations of the 200 MeV  $(p,n)$  transition to the ground state of  $^{13}\text{N}$ .

( $I=0$ ), and complete scattering results are depicted by the long-dashed curves. The tensor and spin-orbit  $t$ -matrix component contributions are displayed by the short-dashed and dot-dashed curves, respectively. In each case the complete  $t$ -matrix result is depicted by the continuous line. Clearly the central and tensor forces give the dominant contributions but the spin-orbit force effects cannot be ignored, especially as there is destructive interference between the matrix elements in the region of  $10^\circ$ – $20^\circ$  ( $0.5 \leq q \leq 1.0 \text{ fm}^{-1}$ ). The  $I=1$  transition probabilities are displayed in the left-hand panel of this figure. At  $0^\circ$  scattering, this differential cross section is due almost solely to the  $1(0,1)$  matrix element and to the central force component of the two-nucleon  $t$  matrix. For scattering angles in excess of  $15^\circ$ , however, not only are the  $1(2,1)$  matrix elements as important but the tensor force gives contributions comparable to those from the central force. Furthermore, there is destructive interference between elements of the calculations. The  $I=0$  transition probabilities are associated with only the  $0(0,0)$  attribute of structure and as evident from the central panel of Fig. 5, get significant contributions from both the central and two-body spin-orbit force components of the two-nucleon  $t$  matrix. The complete results are presented in the right-hand panel of Fig. 5, from which it is evident that the separate central, tensor, and two-body spin-orbit force properties of the  $t$  matrix give significant contributions to the calculations and the interference between their amplitudes is severe.

### B. The $(\frac{3}{2}-\frac{1}{2})$ states

The  $(\frac{3}{2}-\frac{1}{2})$  state in  $^{13}\text{C}$  at 3.68 MeV excitation has an analogue in  $^{13}\text{N}$  at 3.51 MeV excitation energy. Transitions to these states from the  $(\frac{1}{2}-\frac{1}{2})$  ground state in  $^{13}\text{C}$  are specified by the spectroscopic amplitudes given previously in Table IV and have  $M1$ ,  $C2$ , and  $E2$  character. The  $M1$  character is dominantly that of a  $0p_{3/2}$  neutron changing to a  $0p_{1/2}$  specification. But both proton and neutron excitation give important contributions to the  $C2$  and  $E2$  component strengths. For the  $M1$  excitation, isoscalar and isovector spectroscopic amplitudes are comparable, while the  $C2$  and  $E2$  excitations are dominantly

isoscalar in character. It is the isoscalar  $C2$  attribute that most strongly distinguishes the Millener set of values from those of the LK set with  $2h\omega$  components involving excitation out of the  $0p$  shell having spectroscopic amplitudes as much as 10% of the intrashell values.

The  $\frac{3}{2}-\frac{1}{2}$  (3.68 MeV) state was observed in inelastic electron scattering experiments<sup>32</sup> from which both longitudinal and transverse form factors were extracted. Low-energy ( $e, e'$ ) data analysis leads to a  $\gamma$  width of 0.36 eV compared to a resonance fluorescence value<sup>33</sup> of 0.44 eV. Both have an uncertainty of 10% and therefore we used a value of 0.4 eV in extracting the  $B(M1)$  value given in Table V. New data have been measured<sup>38</sup> and are displayed in Figs. 6 and 7, respectively. Therein they are compared with the results of our calculations ( $b = 1.64$ ) made using the LK and Millener spectroscopic amplitudes. In Fig. 6, the longitudinal form factors are presented. It is clear that both calculations are dominated by the isoscalar transition amplitudes and both can be brought into agreement with the magnitude at the maximum by using the enhancement factors for the isoscalar amplitudes found for the  $\gamma$  data and as given in Table VI. The values of  $E_0$  are 1.4 and 1.15 for the LK and Millener cases, respectively, since the latter already has attained much of the needed enhancement in the  $(0+2)h\omega$  space. The form-factor fit could be improved by increasing the oscillator length (to 2 fm). But that is inappropriate since such a large length is not consistent with the value of the root-mean-square charge radius of  $^{13}\text{C}$ . Furthermore, core-polarization corrections are required even with the Millener spectroscopic model and they can be momentum-transfer dependent.<sup>17,36</sup> Thus, use of extraordinarily large values of the oscillator length is problematic [a value of 2.3 fm was required in a recent analysis<sup>5</sup> of  $(p,n)$  data from  $^{14}\text{C}$ ]. The deviation of calculated longitudinal form factors from that specified by the data at high- $q$  values was also observed using Woods-Saxon radial functions<sup>38</sup> with the differences showing a

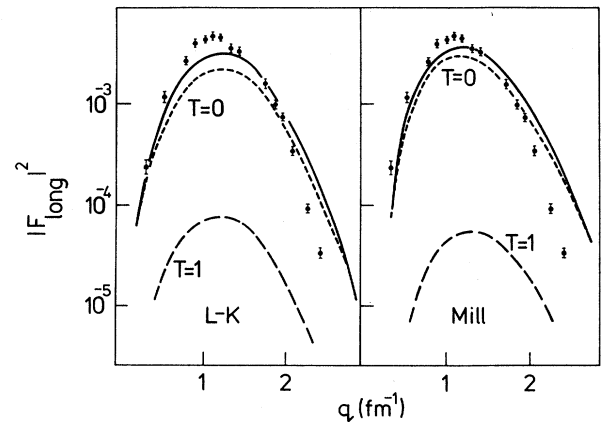


FIG. 6. The longitudinal electron scattering form factor from the excitation of the  $\frac{3}{2}-\frac{1}{2}$  (3.68 MeV) state in  $^{13}\text{C}$ . The data are compared with the calculated results that were obtained using the LK and Millener models of spectroscopy. The separate contributions of isoscalar and isovector components are as indicated.

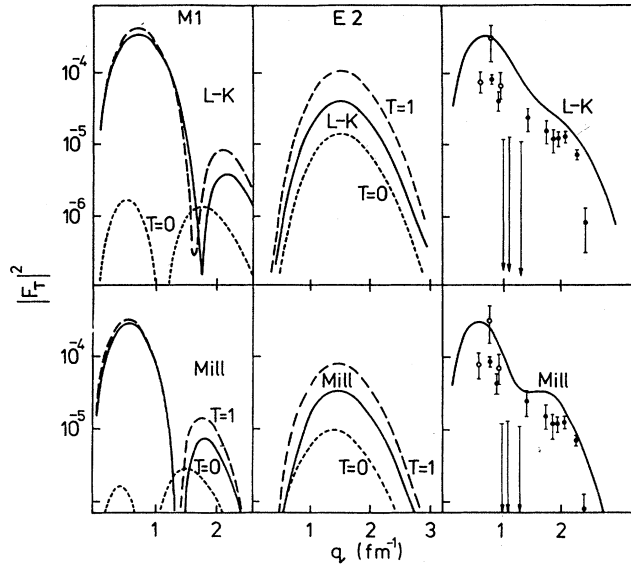


FIG. 7. The transverse form factor from electron scattering to the  $\frac{3}{2}^-\frac{1}{2}$  (3.68 MeV) state in  $^{13}\text{C}$ . The  $M1$  and  $E2$  components that add to give the complete results (shown in the right-hand panel) are compared with the separate isospin transfer contributions.

qualitative similarity to effects of the transition density for the giant quadrupole resonance (GQR) state.

The transverse form factors are shown in Fig. 7, with the  $M1$ ,  $E2$ , and summed results for the LK and Millener (top and bottom) models displayed from left to right. The complete results are compared with the data while the separate contributions (isovector and isoscalar) are displayed for the  $M1$  and  $E2$  parts. It is evident that the isovector  $M1$  contribution dominates the low- $q$  ( $< 1 \text{ fm}^{-1}$ ) predictions, while at higher  $q$  the  $E2$  contribution is the most significant. However, for  $q$  above  $1 \text{ fm}^{-1}$  the destructive interference between isovector and isoscalar contributions is severe. Overall the Millener result is in good agreement with observation considering the sensitivity to details of these evaluations. That sensitivity is shown quite clearly by the results displayed in Fig. 8 wherein the separate  $I(L,S)$  contributions to  $M1$  ( $I=1$ ) form factors are shown. For small momentum-transfer values ( $q < 1 \text{ fm}^{-1}$ ) the  $1(0,1)$  contributions dominate predictions, and are primarily of isovector nature. The  $1(2,1)$  contributions are also predominantly isovector, and are comparable to those of the  $1(0,1)$  set at higher-momentum-transfer values. Contributions from the  $1(1,0)$  elements are minor. But it is clear from the total result, depicted by the continuous curve on the right-hand section of Fig. 8 that there is strong interference between spin 1, monopole ( $L=0$ ), and quadrupole ( $L=2$ ) contributions. Below  $1.5 \text{ fm}^{-1}$  momentum transfer they add constructively but above that value they add destructively.

Despite the considerable sensitivity of the calculated form factors to details in the model of the structure it is apparent that the LK model requires quenching of its isovector  $M1$  components. The  $1(0,1)$  spectroscopic ampli-

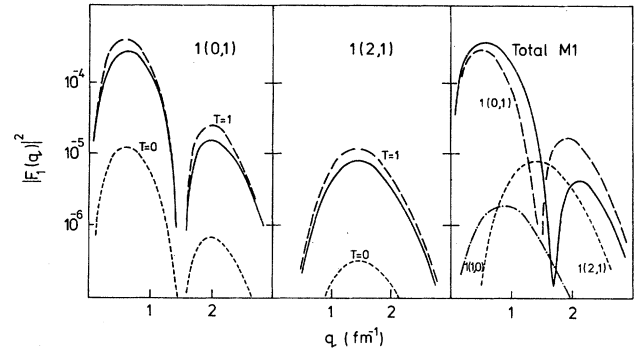


FIG. 8. The component  $I(L,S)$  contributions and their individual isospin transfer parts of the  $M1$  transverse form factor for electron scattering to the  $\frac{3}{2}^-\frac{1}{2}$  (3.68 MeV) state in  $^{13}\text{C}$ . The LK model of spectroscopy was used to obtain the results depicted.

tudes must be substantially reduced. That quenching is not well determined but could be as little as 0.82 or as much as 0.5. More accurate values of the transverse form factors at low momenta are required to improve that estimate, albeit that binding-energy effects<sup>38</sup> may have a significant role in defining quenching at  $0.5 \text{ fm}^{-1}$ .

But other reaction data can be used, to assess these scales. Inelastic proton scattering is a good example since the isospin dependence of ( $p, p'$ ) scattering amplitudes differs from that of the electron scattering form factors. That is quite evident from the results presented in Fig. 9. Therein are shown the results of DWA calculations of the inelastic scattering of 135 MeV protons from  $^{13}\text{C}$  and exciting the  $\frac{3}{2}^-\frac{1}{2}$  (3.68 MeV) state. Those results are compared with the data<sup>18</sup> and were obtained using a phenomenological optical-model potential<sup>18</sup> and the

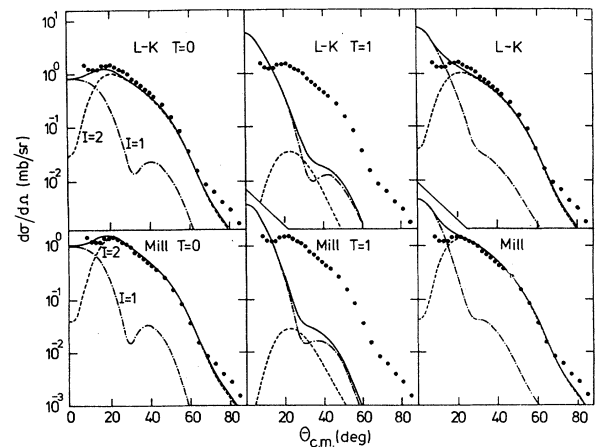


FIG. 9. The 135 MeV ( $p, p'$ ) data from the excitation of the  $\frac{3}{2}^-\frac{1}{2}$  (3.68 MeV) state in  $^{13}\text{C}$  compared with the result of DWA calculations made using the LK (top) and Millener (bottom) transition densities. The separate isoscalar and isovector transition and angular momentum-transfer value components are depicted and are as indicated.

density-dependent Hamburg  $t$  matrix. The results obtained by using the LK model spectroscopic amplitudes are presented in the top section of Fig. 9, while those obtained using the Millener spectroscopic amplitudes are displayed in the bottom section. In both sections, the isoscalar, isovector, and complete results are presented in the left, middle, and right panels, respectively.

The dominant feature of the data is the very characteristic isoscalar  $C2$  and  $E2$  variation; characteristic that is, not only of the angular momentum transfer but also of density dependence (medium corrections) of the two-nucleon  $t$  matrix.<sup>17,18</sup> But the Millener result needs no  $C2$  enhancement and the LK result needs much less than the value of  $E_0$  of 1.46, to fit this data. Thus the composite set of  $\gamma$  decay,  $(e, e')$ , and  $(p, p')$  data analyses are at a variance with regards to this ( $C2$ ) component of the transition density.

As with the transverse electron scattering, the forward scattering  $(p, p')$  data is too sparse to be a sufficiently precise test of the dipole contributions. However, it is quite evident that the dipole spectroscopic amplitudes must be strongly quenched. But now, and unlike the circumstance with the electron scattering transverse form factor, the isoscalar dipole contributions are not negligible. Indeed the isoscalar  $M1$  terms contribute 1 mb/sr at  $0^\circ$  scattering adding almost incoherently to the  $M1$  isovector contribution of 6 mb/sr. Given that the  $t$  matrix is correct, then a reduction of the  $M1$  amplitudes using a value of  $G_1$  in the range 0.5 to 0.8 would give a much improved fit to all of the data. To be more specific more  $(p, p')$  data at smaller scattering angles are required.

But the  $(p, n)$  reaction to the analogue  $\frac{3}{2}^-\frac{1}{2}$  (3.51 MeV) state in  $^{13}\text{N}$  complements the  $(p, p')$  data since only the isovector transition density matrices of Table II are involved in analyses. Very good data, including analyzing power, were obtained recently<sup>5</sup> using 160 MeV polarized protons. In that study, DWIA calculations were reported in which the LK spectroscopy was used in conjunction with the (free) Love-Franey  $t$  matrix. Herein we report on our analyses of that data made using the DWA and with both the LK and Millener models of structure, as well as with the density-dependent Hamburg  $t$  matrices. Our results are compared with the data in Fig. 10. Therein we show the results obtained with the LK and Millener spectroscopies on the left-hand and right-hand sides, respectively. In both cases the small scattering angle region is dominated by transition densities of  $M1$  character. Specifically the  $1(0,1)$  amplitude dominates this component of the transition with contribution from the  $1(2,1)$  rising to about 10% only at the larger ( $\theta_{sc} > 20^\circ$ ) scattering angles. The  $I=2$  contribution is primarily that derived with the  $2(2,1)$  amplitude and is comparable to that of the  $1(0,1)$  amplitude for the larger scattering angles ( $\theta_{sc} > 20^\circ$ ) as well. Clearly, to fit the data for  $\theta_{sc} < 15^\circ$  whatever model of spectroscopy is used, we must quench the isovector  $M1$  amplitudes. The LK result obtained with the density-dependent Hamburg force and from our complete DWA calculation has a value of 20.8 mb/sr at  $0^\circ$  in the center of mass. To compare with the 160 MeV data value of  $10.5 \pm 0.1$  mb/sr then, a value of  $G_1$  of 0.71 is required. We note that our

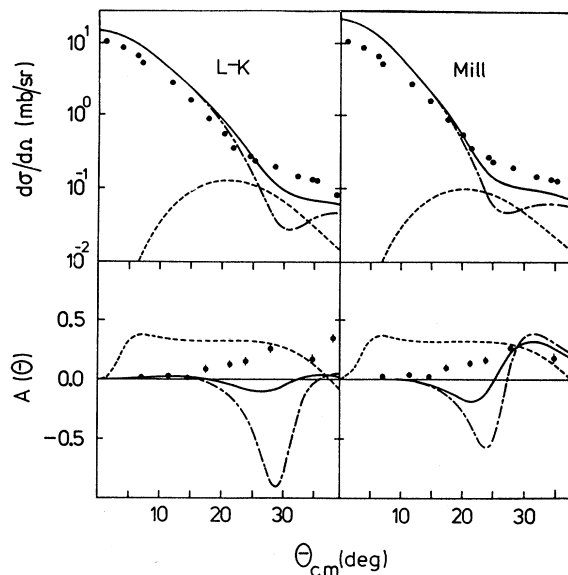


FIG. 10. The 160 MeV data  $(\bar{p}, n)$  from the excitation of the  $\frac{3}{2}^-\frac{1}{2}$  (3.51 MeV) state in  $^{13}\text{N}$  compared with the results of our DWA calculations made using the LK and Millener models of structure. The separate (isovector) angular momentum components are depicted by the dashed ( $I=2$ ) and dash-dotted ( $I=1$ ) curves.

predicted spin-flip probability of 0.63 is in very close agreement with the measured value of  $0.66 \pm 0.02$  as well. Finally, we note again the crucial role of the exchange amplitudes in the DWA. As with the ground-state transition calculated, we find that the exact exchange amplitudes from DWA calculations of this  $\frac{3}{2}^-\frac{1}{2}$  state excitation interfere destructively with those from the direct scattering. Without exchange amplitudes our  $0^\circ$  cross-section value would be 33 mb/sr and so a much larger value of  $G_1$  postulated. Nevertheless  $M1$  quenching is required, and the value of 0.71 for  $G_1$  so determined is in the range of values considered plausible from our analyses of the  $(p, p')$  data.

However, if such  $M1$  quenching is done, then we must enhance the isovector  $I=2$  contributions to give a good representation of the scattering data at scattering angles in excess of  $20^\circ$ . Such an enhancement is indicated by the observed values of the analyzing power. But if we simply scale the isovector  $E2$  transition densities then the electron scattering transverse form factor for  $q > 1 \text{ fm}^{-1}$  would be enhanced and in further disagreement with that data.

To resolve this problem we must study the relative importance of all component contributions to both the  $(p, p')$  and  $(p, n)$  excitation of the  $\frac{3}{2}^-\frac{1}{2}$  states. For 135 MeV  $(p, p')$  of  $^{13}\text{C}$  the various angular momentum transfer component contributions are shown separately in Fig. 11. Of all the possible  $I=1$  contributions only those for which  $(L, S)$  is  $(0, 1)$  are important. The separate central force (short-dashed), two-body spin-orbit force (dash-dotted), and tensor force (long-dashed) contributions are given in all components. Evidently the spin-

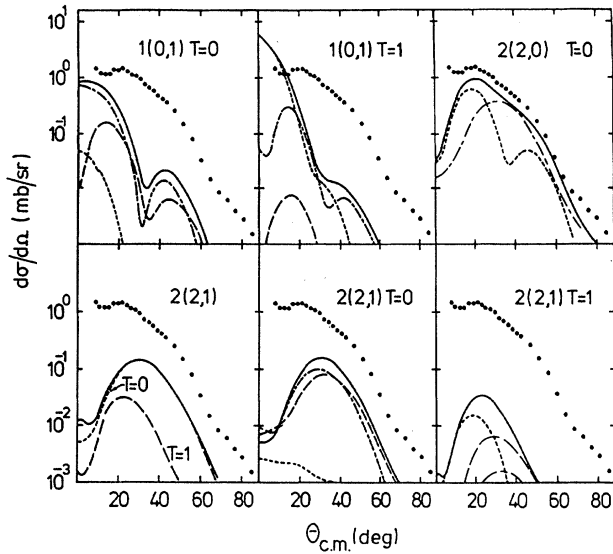


FIG. 11. The most important individual component  $I(LS)$  contributions to DWA calculations of 135 MeV  $(p,p')$  differential cross sections from the excitation of the  $\frac{3}{2}^-$  (3.68 MeV) state in  $^{13}\text{C}$ . In the five panels depicting separate isospin contributions, the central (---), spin orbit (- · - · -), and tensor force (— — —) are displayed. The two isospin and the complete  $2(2,1)$  results are shown in the sixth panel.

orbit and tensor forces contribute strongly to the isoscalar dipole transition whilst it is the central and spin-orbit forces that are most significant for the isovector dipole excitation. As has been noted, this  $1(0,1)$  component dominates the small scattering angle prediction with the isovector strength six times that of the isoscalar strength at  $0^\circ$ . For scattering angles near  $20^\circ$  the isovector and isoscalar  $1(0,1)$  contributions are comparable and by  $30^\circ$  they are both an order of magnitude smaller than the observed data value.

The remaining contributions are for  $I=2$  transfer values with the  $2(2,0)$  and  $2(1,1)$  contributions, the first shown in the right-hand top section of Fig. 11 and being virtually pure isoscalar in nature. The  $2(2,0)$  contribution is clearly the dominant element in the reaction and reflects the observed data variation for scattering angles in excess of  $20^\circ$  in the center of mass. It is important to note that there are no tensor force contributions of significance in this excitation probability. The  $2(1,1)$  contribution is also essentially pure isoscalar, but it is a very small (1%) effect in the total result and so is not displayed. But it is the 10% contributions due to the  $2(2,1)$  components that hold special interest. They are displayed in the bottom of Fig. 11. The isoscalar, isovector, and complete contributions are shown in the left-hand panel while the central, tensor, and two-body spin-orbit force contributions to the isoscalar and isovector excitations are displayed in the middle and right-hand panels, respectively. Clearly the isoscalar excitations part is largest and the isovector contributions, while not insignificant in its own right, changes the result only a little. The exchange amplitudes play a most important role

in these contributions giving strong enhancement upon the direct amplitudes for the isoscalar excitations but strong suppression of the corresponding isovector results.

The isoscalar  $2(2,1)$  contributions are dominated by the tensor and two-body spin-orbit force contributions while in the isovector  $2(2,1)$  calculations it is the central and tensor forces that are most important. But only the isovector  $1(0,1)$  and isovector  $2(2,1)$  probability amplitudes contribute to charge-exchange  $(p,n)$  transition to the analogue of the  $\frac{3}{2}^-$  state at 3.51 MeV in  $^{13}\text{N}$ . Any enhancement of the isovector transition tensor force will thus have minimal effect upon the  $(p,p')$  differential cross section but a substantial change to the  $(p,n)$  predictions. The results of doing so are shown in Fig. 12 and clearly both the  $(p,p')$  and  $(p,n)$  cross-section calculated values are in very good agreement with the data. To obtain these results the  $M1$  isovector spectroscopic amplitudes were all scaled by 0.65 while the tensor force (for the isovector transition only) was multiplied by 1.4. Such an increase in the Hamburg density-dependent (isovector) tensor force is also required to make a consistent analysis<sup>19</sup> of  $(e,e')$ ,  $(\pi^\pm, \pi^\pm)$ ,  $(p,p')$ , and  $(p,n)$  differential cross sections from the excitation of the  $4^-$  states around 19 MeV in  $^{16}\text{O}$ . But the most convincing evidence for this  $t$ -matrix effect is given by the result for the analyzing power that is compared with the data in Fig. 12. The analyzing power is a very sensitive test of details of a reaction calculation, once the differential cross section is fit, since its evaluation involves differences between transition probabilities.

The  $M1$  quenching factor 0.65 is much smaller than accepted by analysis of the  $B(M1)$  value, for example. Furthermore, the forward angle  $(p,n)$  results are then too small in comparison with the data. Indeed it is only the

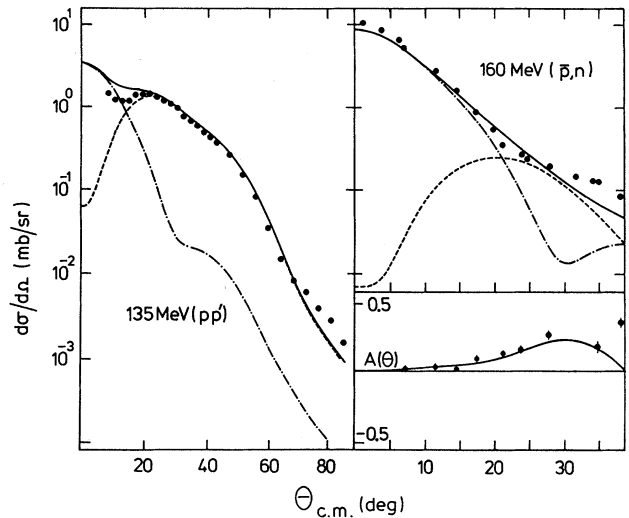


FIG. 12. Simultaneous "best-fit" results for the differential cross sections from 135 MeV  $(p,p')$  and 160 MeV  $(\bar{p},n)$  transitions to the  $\frac{3}{2}^-$  states in  $^{13}\text{C}$  and  $^{13}\text{N}$ , respectively, and to the analyzing power from the charge-exchange reaction. The individual  $I=1$  and  $I=2$  components in the cross section are shown by the dash dotted and dashed curves, respectively.

forward angle ( $p, p'$ ) data that suggest such a reduction factor, and even those data do not extend to very small scattering angles. Clearly more ( $p, p'$ ) data are needed and at even smaller momentum-transfer values before they may be used as a reasonable measure of  $G_1$ .

At higher incident energies, the two-nucleon  $t$  matrix will be less influenced by medium corrections and so the TRIUMF data taken with 200, 300, and 400 MeV protons<sup>1</sup> should be useful tests of our spectroscopy. The results of DWA calculations are compared with the data in Fig. 13. Therein the  $M1$ ,  $E2$ , and complete results for the LK and Millener spectroscopic models are given separately as indicated. In those calculations phenomenological optical-model potentials were used; the parameter values of which were taken from other studies.<sup>13,34</sup> The trend of the data is followed in all cases with both the LK and Millener models of spectroscopy giving  $0^\circ$  cross sections in good agreement with the data, when  $M1$  quenching factors ( $G_1$ ) between 0.7 and 0.8 are used. Thus the degree of quenching ascertained by our analyses of the 160 MeV data is confirmed by these analyses of the higher-energy data. However, we have still used phenomenological optical-model potentials with Schrödinger equations to specify the distorted-wave functions, and there is now a considerable literature on microscopic optical-model potentials as well as of the use of Dirac rather than Schrödinger equations for elastic scattering analyses. We cannot use the latter in our DWA calculations (fully antisymmetrized version) but microscopic optical potentials can be used. Such potentials for carbon have been generated<sup>35</sup> using the Hamburg  $t$  matrices and at 200, 300, and 400 MeV. Their use gave ( $p, n$ ) cross sections quite similar to those obtained using the phenomenological potentials but usually smaller in overall magnitude. The results for 200, 300, and 400 MeV using the MOP potentials, and scaled to fit the  $0^\circ$  cross-section data are as delineated in Fig. 14. The 400 MeV MOP result is shown again in comparison with the phenomeno-

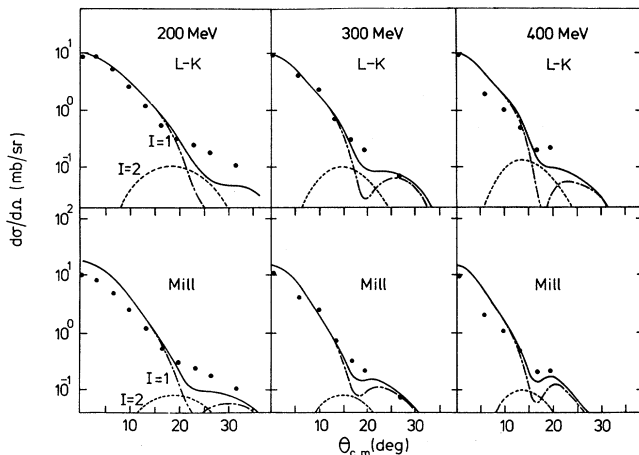


FIG. 13. A comparison of the results of DWA calculations with data from the ( $p, n$ ) excitation of the  $\frac{3}{2}^-$  state at 3.51 MeV in  $^{13}\text{N}$ . At each incident energy the individual angular momentum-transfer contributions are shown and for both the LK and Millener spectroscopic models.

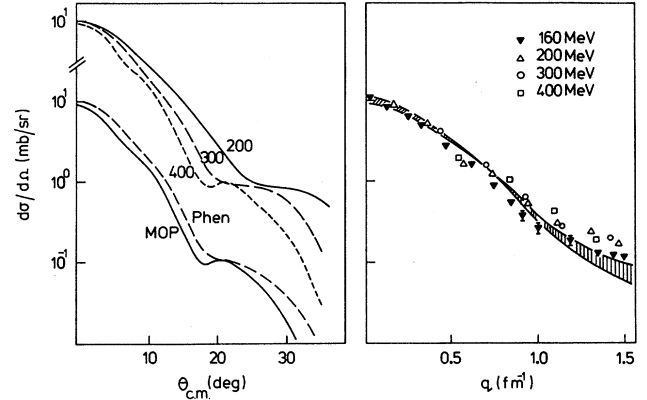


FIG. 14. Left: The DWA results for the ( $p, n$ ) transition to the  $\frac{3}{2}^-$  ( $3.51$  MeV) state in  $^{13}\text{N}$  at the different energies specified and obtained using microscopic optical-model potentials (MOP). Right: All of the ( $p, n$ ) data from the excitation of the  $\frac{3}{2}^- \rightarrow \frac{1}{2}^-$  ( $3.51$  MeV) state in  $^{13}\text{N}$  compared with the range of calculated values as given by our DWA calculations.

logical potential result to stress the differences. But it is the scaling to fit the  $0^\circ$  value of the differential cross sections that is the most interesting. The results displayed have all used  $G_1$  with a value of 0.84 to give  $0^\circ$  cross-section values of 10, 10, and 9 mb/sr at the energies of 200, 300, and 400 MeV, respectively.

On the right-hand side of Fig. 14, the 160, 200, 300, and 400 MeV data are plotted as functions of momentum transfer and we compare that hadronic form factor with the range of values as given by the 200, 300, and 400 MeV (MOP) calculations. In this representation it is evident that the LK spectroscopy with the Hamburg  $t$  matrix and microscopically generated optical-model potentials give a very good representation of the totality of the data.

### C. The $\frac{3}{2}^- - \frac{3}{2}^-$ states

The first  $T = \frac{3}{2}$  state in  $^{13}\text{C}$  has a spin parity of  $\frac{3}{2}^-$  and an excitation energy of 15.11 MeV. It also has an analogue in  $^{13}\text{N}$  at an energy of 15.07 MeV. Excitation of these states from the  $^{13}\text{C}$  ground state are purely isovector in nature with spectroscopic amplitudes being known from the LK and Singham models of spectroscopy. Those amplitudes are listed in Table VII and from which the  $j$ - $j$  representation values can be specified by using Eqs. (6) and (8). The Singham values are then smaller than those of the LK set reflecting the smaller values of the  $B(M1)$  and  $B(C2)$  we obtained previously.

The earliest experimental studies by inelastic electron scattering<sup>32</sup> extracted  $M1$  and  $C2$  decay widths and Petersen<sup>37</sup> observed that the  $M1$  decay rate was consistent with the  $\beta$  decay of  $^{13}\text{B}$  (to the  $^{13}\text{C}$  ground state) when a  $\log ft$  of 4.01 is assumed. Both the LK and Singham models of spectroscopy give results in good agreement with the data, the former with the canonical value of 0.9 for the suppression factor,  $G_1$ .

Data now exist from which the electron scattering transverse form factor has been measured<sup>28,38</sup> to a

momentum transfer of  $2.8 \text{ fm}^{-1}$ . That composite set of data is shown in Fig. 15 and is compared therein with our calculated results. The complete ( $M1$  plus  $E2$ ) form factors from the LK and Singham models of spectroscopy are presented by the continuous lines, while the separate  $M1$  and  $E2$  contributions using Singham's prescription are shown by the short-dashed and long-dashed lines, respectively. As noted by Singham,<sup>28</sup> by adjusting the  $Op_{1/2}$  strength in the LK wave functions, the resulting form factor is smaller and thereby in better agreement with the data. But then one is faced with the question of how the "new" ground-state prescription will influence other transitions, and what form of two-body potentials would be required to give that new ground-state function.

From Fig. 15 it is clear that the LK spectroscopic amplitudes must be quenched if a good fit to the measured data is to be obtained. In the vicinity of  $1.7 \text{ fm}^{-1}$  momentum transfer only the isovector  $E2$  contribution to the form factor is significant and so an isovector  $E2$  quenching of 0.7 (to the amplitudes) is necessary. At lower- $q$  values the  $M1$  and  $E2$  contributions are both important (albeit the  $M1$  dominates) whence an  $M1$  suppression of 0.9 (for  $G_1$ ) suffices to give a fit to data when the 70%  $G_2$  quenching is used. This  $M1$  quenching is consistent with the fit to the  $B(M1)$  value. But no account has been made of the effects found using Woods-Saxon wave functions.<sup>38</sup>

The  $\frac{3}{2}^{\pm}\frac{3}{2}^{\pm}$  state excitation has been measured by the inelastic scattering of 135 MeV protons,<sup>18</sup> and in Fig. 16, those data are compared with results of DWA calculations made using the LK spectroscopy but adjusting the suppression factors  $G_1$  and  $G_2$  to obtain a good fit. The separate  $I=1$  and  $I=2$  contributions obtained using the Hamburg density-dependent force are displayed by the

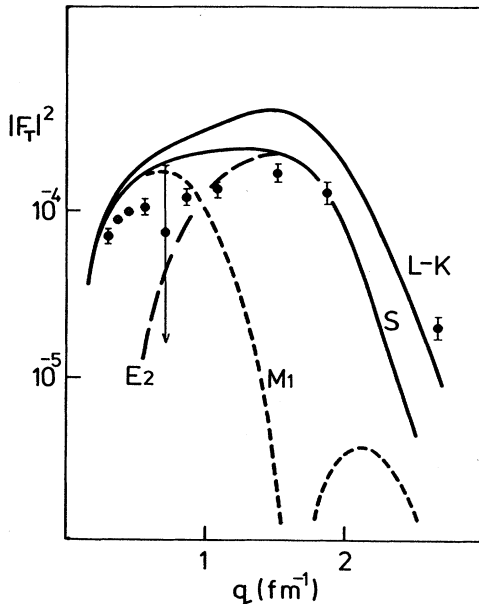


FIG. 15. The transverse form factor from electron scattering to the  $\frac{3}{2}^{\pm}\frac{3}{2}^{\pm}$  (15.11 MeV) state in  $^{13}\text{C}$ . The calculated results were obtained using the LK and Singham models of spectroscopy.

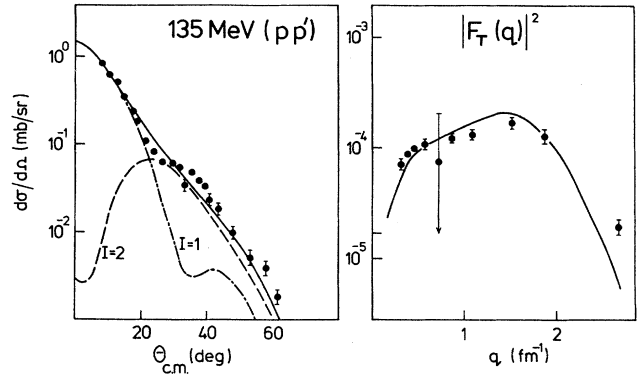


FIG. 16. Proton and electron scattering data from the excitation of the  $\frac{3}{2}^{\pm}\frac{3}{2}^{\pm}$  state at 15.11 MeV in  $^{13}\text{C}$  and compared with calculations made using quenched spectroscopic amplitudes.

dot-dashed and dashed curves, respectively. The required  $G_2$  quenching was 0.7 in agreement with the foregoing discussion but the  $G_1$  value is now 0.7 as well. With those suppression factors the electron scattering form-factor prediction is that shown by the continuous curve in the right-hand panel in Fig. 16. Clearly the low- $q$  form factor is now too small and the  $B(M1)$  prediction would be also.

In this instance, enhancing the tensor force strength by 40% makes matters worse. The same fit to the  $(p,p')$  cross-section data can be obtained but the suppression factors change to  $G_1=0.65$  and  $G_2=0.58$ . Clearly there is an incompatibility between the data analyses. But there is one other piece of datum we can use and that is the differential cross section (and spin-flip probability) at  $0^\circ$  for the charge-exchange ( $\bar{p},n$ ) transition. The measurement gave values of  $2.7 \pm 0.2 \text{ mb/sr}$  and  $0.68 \pm 0.4$  for these quantities. From our DWA calculations we observe now only the dominance of the  $1(0,1)$  contribution but also the important destructive interference of the exchange amplitudes. Specifically, and with  $G_1$  of 0.71, the purely direct scattering calculation gave a cross section of  $4.36 \text{ mb/sr}$  with a spin-flip probability of 0.67. Inclusion of the exchange amplitudes reduced those values of  $2.75 \text{ mb/sr}$  and 0.63, respectively, also giving good agreement with the measured data. On face value we have a dichotomy over the value of  $G_1$  required for electromagnetic and hadron scattering; and one which seems independent of our choice of radial wave functions. However, it remains to be seen just how different results become with the use of more realistic single-particle bound-state wave functions. Even so, more, and accurately measured, hadron scattering data at low- $q$  values especially are required to proceed.

#### IV. CONCLUSIONS

The properties of the  $^{13}\text{C}$  ( $^{13}\text{N}$ ) ground states and the transitions between them have been measured very accurately. Predictions of those properties obtained using  $Op$  shell models of nuclear structure, as well with those in which  $2h\omega$  excitations upon the  $Op$  shell limited basis

space were allowed, are all very similar. However, only the latter, with an  $M1$  suppression factor of 0.82 to the  $1(0,1)$  isovector amplitudes gave a fit to the magnetic moment difference as well as to the  $B_{GT}$  from  $\beta$  decay. But for momentum-transfer values  $q$  up to  $0.8 \text{ fm}^{-1}$ , no such  $M1$  suppression is needed to fit both the transverse electron scattering form factor and the range of  $(p,n)$  data taken with 160–400 MeV protons. The latter data analyses were made in the DWA using the complex, energy- and density-dependent Hamburg  $t$  matrices and fully antisymmetrized scattering states. For larger momentum-transfer values no calculation reproduces the data variation; the very high- $q$  ( $\geq 3 \text{ fm}^{-1}$ ) electron scattering form factor is most unusual. But in the region  $1\text{--}2 \text{ fm}^{-1}$  the isoscalar and isovector contributions to the electron scattering form factor interfere destructively and also multi- $h\omega$  corrections have a most drastic effect. The latter corrections seem to have similar large effects upon calculations of the differential cross sections for the  $(p,n)$  reaction.

The essential result is that  $\beta$  decay and magnetic moments ( $q=0$  data) are fit with a renormalization ( $G_1=0.82$ ) of the structure models but, as is stressed by the comparison shown in Table X, little or no quenching is required to fit both the transverse electron scattering form factor and the intermediate energy  $(p,n)$  hadronic form factor to a momentum transfer of  $0.8 \text{ fm}^{-1}$ . It remains to be seen whether or not a much larger basis model of structure would so alter contributions that the form factors would be markedly changed to give fits to data for  $q > 1 \text{ fm}^{-1}$  and also so vary the predicted values for  $q < 1 \text{ fm}^{-1}$  that all data be fit concomitantly. Indeed, we note that the interference between components to the electron scattering form factor could permit a value of  $G_1$  consistent with the  $\beta$ -decay requirement.

The first excited ( $\frac{3}{2}\text{--}\frac{1}{2}$ ) states decay to the ground via  $M1$  and  $C2$   $\gamma$ -ray emission with transition probabilities that measure a mixture of  $S_{1(01)}^{(7)}$  and  $S_{1(10)}^{(7)}$  spectroscopic amplitudes and those of  $S_{2(20)}^{(7)}$ , respectively. The  $0p$  shell-model  $B(M1)$  values match the data when a suppression factor ( $G_1$ ) of 0.82 is applied whereas to match the observed  $B(C2)$  value an enhancement of isoscalar  $2(2,0)$  amplitudes of 1.46 is required. With the  $2h\omega$  additions, the Millener wave functions give transition densities for which the values of  $G_1$  and  $E_0$  need be 0.79 and 1.16, respectively.

The  $C2$  enhancement is confirmed in the analyses of the longitudinal electron scattering form factor but the intermediate energy (135 MeV) inelastic proton scattering data needs much less to fit data in the  $20^\circ\text{--}60^\circ$  region. Likewise, the transverse form factor from electron scattering, the forward angle ( $q < 0.8 \text{ fm}^{-1}$ ) inelastic proton scattering data, and the set of  $(p,n)$  data shows that the shell-model  $M1$  spectroscopic amplitudes  $S_{1(01)}^{(7)}$  need to be quenched. But the inelastic scattering data are too sparse in the low- $q$  region to define  $G_1$  other than to a range of 0.5 to 0.8. For  $q > 1 \text{ fm}^{-1}$ , the electron scattering form factor is dominantly that of  $E2$  character and a reduction factor  $G_2$  of 0.8 would also give a good fit to the data. But the isoscalar and isovector transition contributions interfere destructively, so that a slight variation in their relative importance may be all that is needed to reproduce the observed values. Indeed, with  $G_1$  of 0.65 and an increased isovector tensor force the 135 MeV  $(p,p')$  differential cross section, the 160 MeV  $(p,n)$  differential cross section, and analyzing power are all fit very well, albeit that the  $0^\circ$   $(p,n)$  result is low. The mix, however, is necessary to get the amount of  $E2$  contribution needed to reproduce the analyzing power data.

From Table X it is obvious that our analyses of the  $(p,n)$  data taken with 200, 300, and 400 MeV confirm that a significant quenching, with  $G_1$  of 0.7–0.8, is necessary for the  $M1$  component of either model of spectroscopy. Smaller  $q$  data from the (transverse)  $(e,e')$  and  $(p,p')$  reactions are needed to be more definitive.

Finally, we have analyzed data from the excitation of the ( $\frac{3}{2}\text{--}\frac{3}{2}$ ) states. For this the measured  $B(M1)$  for  $\gamma$  decay to ground and the  $\beta$  decay of  $^{13}\text{B}$  are given as calculated when the  $0p$  shell-model spectroscopic amplitude  $S_{1(01)}^{(1)}$  is quenched using  $G_1$  of 0.9. No variation is required to the calculated isovector  $C2$  and  $E2$  amplitudes. But, as with the ground-state transitions, the inelastic electron scattering form factor requires suppression of both calculated  $M1$  (by 0.9) and  $E2$  (by 0.7) amplitudes to get agreement between the  $0p$  shell-model predictions and data. The inelastic proton scattering cross-section data are fit essentially with the same  $E2$  reduction but need a larger suppression (0.7) of the  $M1$  component. The  $(p,n)$  data have not been extracted from the spectra as yet<sup>1</sup> and it will be of interest to discover if that finite  $q$  data also indicate quenching in excess of the values deemed appropriate from the  $\beta$ - and  $\gamma$ -decay transition rate analy-

TABLE X.  $M1$  quenching factors,  $G_1$ .

	$\frac{1}{2}\text{--}\frac{1}{2}$		$\frac{3}{2}\text{--}\frac{1}{2}$		$\frac{3}{2}\text{--}\frac{3}{2}$
	LK	Millener	LK	Millener	LK
Moments	0.92	0.82			
$B_{GT}$	0.80	0.82			0.9
$B(M1)$			0.8	0.8	0.9
$(e,e')$ tran.	1.0	0.9–1.0	0.5–0.8	0.5–0.8	0.9 <sup>a</sup>
135 $(p,p')$			0.5–0.8	0.5–0.8	0.65–0.7
160 $(p,n)$	1.0	1.0	0.71	0.7	0.71
200–400 $(p,n)$	1.0	1.0	0.7–0.84	0.7–0.84	

<sup>a</sup>When an  $E2$  quenching of 0.7 is also used.

ses. Of the three transitions considered, analyses of the  $\frac{3}{2}-\frac{3}{2}$  state excitations are the least consistent. With an "improved" isovector tensor force  $t$  matrix, proton inelastic scattering data analyses require even larger suppressions of the spectroscopic amplitudes. But, it is to be remembered that there is a marked interference between the contributing matrix elements to the transverse (electron scattering) form factor, and a marked (destructive) interference between direct and exchange proton scattering amplitudes for the excitation of the  $\frac{3}{2}-\frac{3}{2}$  state. Destructive interference effects are hard to specify accurately.

Clearly the "complete" data set of  $\beta$ - and  $\gamma$ -ray-rates, electron scattering form factors and intermediate energy ( $p, p'$ ) and ( $p, n$ ) reaction data make stringent and complementary tests of models of nuclear structure. For the  $^{13}\text{C}$  transitions considered such a complete set requires as yet more measurements of ( $e, e'$ ) form factors and ( $p, p'$ ) excitations and in the kinematic regions of momentum transfer between 0 and  $0.5 \text{ fm}^{-1}$ , especially for the latter. With such data either the  $0p$  shell quenching may be resolved or a dichotomy of the reaction and/or structure models defined. It is encouraging to observe, however, that any Nilsson projected estimate for corrections to  $0p$  shell-model structure of the state of  $^{13}\text{C}$  gives a suppression of matrix elements of operation of  $(Y_2 \times \sigma_1)^\lambda$  type. A different  $G_1$  scaling may then be expected for  $M1$  effects at different values of momentum transfer and for

different reaction mechanisms when the simple  $0p$  shell model is used in analyses. Such is also anticipated in view of the marked effects in form-factor predictions observed<sup>38</sup> using Woods-Saxon rather than harmonic-oscillator radial wave functions.

Finally, we have established how one should analyze ( $p, n$ ) data at  $0^\circ$  scattering angle (and at all others) to extract  $B_{GT}$  values. At the very least a complete, properly antisymmetrized, DWA calculation using pertinent complex, energy- and density-dependent two-nucleon  $t$  matrices must be made since exchange amplitudes can have serious interference effects with the direct ones, and the  $t$ -matrix components and strengths are crucial in obtaining absolute magnitudes of cross sections. Only then may one hope to assess realistic scale variations upon the transition spectroscopic amplitudes,  $S_{I(LS)}$ , for example, and which are required in calculations of  $\beta$ - and  $\gamma$ -decay rates.

#### ACKNOWLEDGMENTS

We are most grateful to the TRIUMF Collaboration for providing their ( $p, n$ ) data prior to publication, and to Professor W. P. Alford of that collaboration for a number of suggestions of value to this work. We are also most grateful to Professor D. J. Millener for the many incisive comments about the material and presentation that he provided in assistance to us.

\*On leave from Argonne National Laboratory, Argonne, IL 60439.

- <sup>1</sup>T. N. Taddeucci, T. A. Carey, C. Gaarde, J. Larsen, C. D. Goodman, D. J. Horen, T. Masterson, J. Rapaport, T. P. Welch, and E. Sugarbaker, *Phys. Rev. Lett.* **52**, 1960 (1984); T. N. Taddeucci, C. A. Goulding, T. A. Carey, R. C. Byrd, C. D. Goodman, C. Gaarde, J. Larsen, D. Horen, J. Rapaport, and E. Sugarbaker, *Nucl. Phys.* **A469**, 125 (1987); C. D. Goodman, *Comments Nucl. Part. Phys.* **10**, 117 (1981); C. D. Goodman, R. C. Byrd, I. J. Van Heerden, T. A. Carey, D. J. Horen, J. S. Larsen, C. Gaarde, J. Rapaport, T. P. Welch, E. Sugarbaker, and T. N. Taddeucci, *Phys. Rev. Lett.* **54**, 877 (1985); W. P. Alford, R. L. Helmer, R. Abegg, A. Celler, O. Häusser, K. Hicks, K. P. Jackson, C. A. Miller, S. Yen, R. E. Azuma, D. Freckers, R. S. Henderson, H. Baer, and C. D. Zafiratos, *Phys. Lett. B* **179**, 20 (1986); W. P. Alford *et al.* (unpublished).
- <sup>2</sup>C. D. Goodman, C. A. Goulding, M. B. Greenfield, J. Rapaport, D. E. Bainum, C. C. Foster, W. G. Love, and F. Petrovich, *Phys. Rev. Lett.* **44**, 1755 (1980).
- <sup>3</sup>J. W. Watson, W. Pairsuan, B. D. Anderson, A. R. Baldwin, B. S. Flanders, R. Madey, R. J. McCarthy, B. A. Brown, B. H. Wildenthal, and C. C. Foster, *Phys. Rev. Lett.* **55**, 1369 (1985).
- <sup>4</sup>W. G. Love, K. Nakayama, and M. A. Franey, *Phys. Rev. Lett.* **59**, 1401 (1987).
- <sup>5</sup>J. N. Rapaport, D. Wang, J. A. Carr, F. Petrovich, C. C. Foster, C. D. Goodman, C. Gaarde, J. Larsen, C. A. Goulding, T. N. Taddeucci, D. Horen, and E. Sugarbaker, *Phys. Rev. C* **36**,

- 500 (1987).
- <sup>6</sup>N. S. P. King, P. W. Lisowski, G. L. Morgan, P. N. Craig, R. G. Jeppesen, D. A. Lind, J. R. Shepard, J. L. Ullmann, C. D. Zafiratos, C. D. Goodman, and C. A. Goulding, *Phys. Lett. B* **175**, 279 (1986).
- <sup>7</sup>C. J. Horowitz, *Phys. Lett. B* **196**, 285 (1987).
- <sup>8</sup>A. Picklesimer, P. C. Tandy, and R. M. Thaler, *Phys. Rev. C* **25**, 1215 (1982).
- <sup>9</sup>W. G. Love, and M. A. Franey, *Phys. Rev. C* **24**, 1073 (1981).
- <sup>10</sup>M. H. MacFarlane and E. F. Redish, *Phys. Rev. C* **37**, 2245 (1988).
- <sup>11</sup>F. A. Brieva and J. R. Rook, *Nucl. Phys.* **A291**, 219 (1987); **A291**, 317 (1977).
- <sup>12</sup>H. V. von Geramb and K. Nakano, in *The Interaction Between Medium Energy Nucleons and Nuclei (Indiana, 1982)* Proceedings of the Workshop on the Interaction Between Medium Energy Nucleons in Nuclei, AIP Conf. Proc. No. 97, edited by H. O. Meyer (AIP, New York, 1983).
- <sup>13</sup>L. Rikus, K. Nakano, and H. V. von Geramb, *Nucl. Phys.* **A414**, 413 (1984).
- <sup>14</sup>E. F. Redish and K. Stricker-Bauer, *Phys. Rev. C* **35**, 1183 (1987); K. Amos, L. Berge, F. A. Brieva, A. Katsogiannis, L. Petris, and L. Rikus, *ibid.* **37**, 934 (1988).
- <sup>15</sup>J. Raynal, program DWBA82, Centre d'Etudes Nucleaires de Saclay (Gif-Sur-Yvette, France) (unpublished).
- <sup>16</sup>M. Lacombe, B. Loiseau, J. M. Richard, R. Vinh Mau, J. Côté, P. Pirès, and R. de Tourreil, *Phys. Rev. C* **21**, 861 (1980).
- <sup>17</sup>K. Amos and W. Bauhoff, *Nucl. Phys.* **A424**, 60 (1984); M.

- Hugi, W. Bauhoff, and H. O. Meyer, *Phys. Rev. C* **28**, 1 (1983).
- <sup>18</sup>S. F. Collins, G. G. Shute, B. M. Spicer, V. C. Officer, I. Morrison, K. A. Amos, D. W. Devins, D. L. Friesel, and W. P. Jones, *Nucl. Phys.* **A380**, 445 (1982); S. F. Collins, G. G. Shute, B. M. Spicer, V. C. Officer, D. W. Devins, D. L. Friesel, and W. P. Jones, *ibid.* **A481**, 494 (1987).
- <sup>19</sup>L. Berge, Ph.D. thesis, University of Melbourne, 1988.
- <sup>20</sup>S. Cohen and D. Kurath, *Nucl. Phys.* **73**, 1 (1965); D. J. Millener and D. Kurath, *Phys. Rev. A* **255**, 315 (1975).
- <sup>21</sup>T.-S.H. Lee and D. Kurath, *Phys. Rev. C* **21**, 293 (1980).
- <sup>22</sup>T. Suzuki, H. Hyuga, A. Arima, and K. Yakazi, *Nucl. Phys.* **A358**, 421C (1981); K. Shimuzu, M. Ichimura, and A. Arima, *ibid.* **A226**, 282 (1974).
- <sup>23</sup>I. S. Towner and F. C. Khanna, *Nucl. Phys.* **A399**, 334 (1983).
- <sup>24</sup>P. G. Blunden and B. Castel, *Nucl. Phys.* **A445**, 742 (1985).
- <sup>25</sup>R. S. Hicks, J. Dubach, R. A. Lindgren, B. Parker, and G. A. Peterson, *Phys. Rev. C* **26**, 339 (1982); R. S. Hicks, R. L. Huffman, R. A. Lindgren, G. A. Peterson, M. A. Plum, and J. Button-Shafer, *ibid.* **36**, 485 (1987).
- <sup>26</sup>D. J. Millener (unpublished).
- <sup>27</sup>E. K. Warburton, D. E. Alburger, and D. J. Millener, *Phys. Rev. C* **22**, 2330 (1980).
- <sup>28</sup>M. K. Singham, *Phys. Rev. Lett.* **54**, 1642 (1985); Erratum *Phys. Rev. Lett.* **55**, 1156 (1985).
- <sup>29</sup>I. T. Cheon, *Phys. Lett.* **124B**, 451 (1983).
- <sup>30</sup>D. H. Wilkinson, *Nucl. Phys.* **A209**, 470 (1973).
- <sup>31</sup>D. H. Wilkinson, *Nucl. Phys.* **A377**, 474 (1982).
- <sup>32</sup>G. Wittwer, H.-G. Clerc, and G. A. Beer, *Phys. Lett.* **30B**, 634 (1969).
- <sup>33</sup>S. W. Robinson, C. P. Swann, and V. K. Rasmussen, *Phys. Lett.* **26B**, 298 (1968).
- <sup>34</sup>H. O. Meyer, P. Schwandt, G. L. Moake, and P. P. Singh, *Phys. Rev. C* **23**, 616 (1981); H. O. Meyer, P. Schwandt, R. Abegg, C. A. Miller, K. P. Jackson, S. Yen, G. Gaillard, M. Hugi, R. Helmers, D. Frekers, and A. Saxena, *ibid.* **37**, 544 (1988).
- <sup>35</sup>H. V. von Geramb (private communication).
- <sup>36</sup>K. Amos and L. Berge, *Phys. Lett.* **127B**, 299 (1983).
- <sup>37</sup>G. A. Peterson, *Phys. Lett.* **25B**, 549 (1967).
- <sup>38</sup>D. J. Millener, D. I. Sober, H. Crannell, J. T. O'Brien, L. W. Fagg, S. Kowalski, C. F. Williamson, and L. Lapikás, *Phys. Rev. C* **39**, 14 (1989).
- <sup>39</sup>F. Ajzenberg-Selove, *Nucl. Phys.* **A360**, 1 (1981); **A449**, 1 (1986).
- <sup>40</sup>R. E. Marrs, E. G. Adelberger, K. A. Snover, and M. D. Cooper, *Phys. Rev. Lett.* **35**, 202 (1975).